

1
2
3
4
5
6
7
8
9
10
11
12
13
14
15
16
17
18
19
20
21
22
23
24
25
26
27
28
29

Biomass Burning Aerosols and the Low Visibility Events in Southeast Asia

Hsiang-He Lee^{1@}, Rotem Z Bar-Or², and Chien Wang^{1,2}

¹Center for Environmental Sensing and Modeling, Singapore-MIT Alliance for Research
and Technology, Singapore

²Center for Global Change Science, Massachusetts Institute of Technology, Cambridge,
MA, U.S.A.

Submitted to
Atmospheric Chemistry and Physics

June 14, 2016

[@]Corresponding author address: Dr. Hsiang-He Lee, 1 CREATE Way, #09-03 CREATE
Tower, Singapore, 138602
E-mail: hsiang-he@smart.mit.edu

30 **Abstract**

31 Fires including peatland burning in Southeast Asia have become a major concern to
32 the general public as well as governments in the region. This is because aerosols emitted
33 from such fires can cause persistent haze events under certain weather conditions in
34 downwind locations, degrading visibility and causing human health issues. In order to
35 improve our understanding of the spatial-temporal coverage and influence of biomass
36 burning aerosols in Southeast Asia, we have used surface visibility and particulate matter
37 concentration observations, supplemented by decadal long (2003 to 2014) simulations
38 using the Weather Research and Forecasting (WRF) model with a fire aerosol module,
39 driven by high-resolution biomass burning emission inventories. We find that in the past
40 decade, fire aerosols are responsible for nearly all the events with very low visibility (<
41 7km). Fire aerosols alone are also responsible for a substantial fraction of the low
42 visibility events (visibility < 10 km) in the major metropolitan areas of Southeast Asia:
43 up to 39% in Bangkok, 36% in Kuala Lumpur, and 34% in Singapore. Biomass burning
44 in mainland Southeast Asia account for the largest contribution to total fire-produced
45 PM_{2.5} in Bangkok (99%), while biomass burning in Sumatra is a major contributor to fire-
46 produced PM_{2.5} in Kuala Lumpur (50%) and Singapore (41%). To examine the general
47 situation across the region, we have further defined and derived a new integrated metric
48 for 50 cities of the Association of Southeast Asian Nations (ASEAN): the Haze Exposure
49 Day (HED), which measures the annual exposure days of these cities to low visibility (<
50 10 km) caused by particulate matter pollution. It is shown that HEDs have increased
51 steadily in the past decade across cities with both high and low populations. Fire events
52 alone are found to be responsible for up to about half of the total HEDs. Our results

53 suggest that in order to improve the overall air quality in Southeast Asia, mitigation
54 policies targeting both biomass burning and fossil fuel burning sources need to be
55 implemented.

56 **1 Introduction**

57 In recent decades, biomass burning has become frequent and widespread across
58 mainland Southeast Asia and the islands of Sumatra and Borneo (Langner et al., 2007;
59 Carlson et al., 2012; Page et al., 2002; van der Werf et al., 2010). Abundant aerosols
60 emitted from such fires cause haze events to occur in downwind locations such as
61 Singapore (Koe et al., 2001; Heil et al., 2007; See et al., 2006), degrading visibility and
62 threatening human health (Emmanuel, 2000; Kunii et al., 2002; Johnston et al., 2012;
63 Mauderly and Chow, 2008; Crippa et al., 2016). Besides causing air quality issues, the
64 fire aerosols contain rich carbonaceous compounds such as black carbon (BC) (Fujii et
65 al., 2014) and thus can reduce sunlight through both absorption and scattering. Indirect
66 effects of fire aerosols on the climate are even more complicated due to various cloud
67 types and meteorological conditions in the Maritime Continent (MC) (Sekiguchi et al.,
68 2003; Lin et al., 2013; Wu et al., 2013; Grandey et al., 2016).

69 The majority of present day fires in Southeast Asia occur due to human interference
70 such as land clearing for oil palm plantations, other causes of deforestation, poor peatland
71 management, and burning of agriculture waste (Dennis et al., 2005; Marlier et al., 2015a).
72 Certain policies and regulations, such as those regarding migration, also affect the
73 occurrence of burning events. Large fires have occurred since the 1960s in Sumatra;
74 however, the first fire event in Kalimantan happened in the 1980s (Field et al., 2009).
75 Based on economic incentives and population growth in Southeast Asia, future land-use
76 management will play an important role in determining the occurrence of fires across the
77 region (Carlson et al., 2012; Marlier et al., 2015b).

78 Besides human interventions, meteorological factors can also influence fire
79 initiation, intensity, and duration (Reid et al., 2012; Reid et al., 2015). Of particular
80 importance is rainfall. Reid et al. (2012) investigated relationships between fire hotspot
81 appearance and various weather phenomena as well as climate variabilities in different
82 time scales over the MC, including: (1) the El Niño-Southern Oscillation (ENSO)
83 (Rasmusson and Wallace, 1983; McBride et al., 2003) and the Indian Ocean Dipole
84 (IOD) (Saji et al., 1999); (2) seasonal migration of the Inter-tropical Convergence Zone
85 (ITCZ) and associated Southeast Asia monsoons (Chang et al., 2005); (3) intra-seasonal
86 variability associated with the Madden-Julian Oscillation (MJO) (Madden and Julian,
87 1971; Zhang, 2005) and the west Sumatran low (Wu and Hsu, 2009); (4) equatorial
88 waves, mesoscale features, and tropical cyclones; and (5) convection. One interesting
89 finding is that the influence of these factors on fire events varies over different parts of
90 the MC. For example, the fire signal in one part of Kalimantan is strongly related to both
91 the monsoons and ENSO. In contrast, fire activity in Central Sumatra is closely tied to
92 neither the monsoons nor ENSO, but is closely tied to the MJO.

93 Climate variability of meteorological phenomena affects not only biomass burning
94 emissions but also transport of fire aerosols (Reid et al., 2012). The seasonal migration
95 of the ITCZ and the associated monsoonal circulation dominate seasonal wind flows,
96 whereas sea breezes, tropical cyclones, and topography determine air flow on smaller
97 spatial and temporal scales – all these phenomena play significant roles in determining
98 the transport pathway of fire aerosols (Wang et al., 2013). For example, the intense haze
99 episode of June 2013, a long lasting event with a “very unhealthy” air pollution level in
100 Singapore, was actually caused by enhanced fire aerosol transport from Sumatra to West

101 Malaysia owing to a tropical cyclone located in South China Sea. Recently, using a
102 global chemistry transport model combined with a back-trajectory tracer model,
103 Reddington et al. (2014) attempted to attribute particulate pollution in Singapore to
104 different burning sites in surrounding regions over a short time period of 5 years. The
105 coarse 2.8-degree resolution model used in the study, however, has left many open
106 questions.

107 In this study, we aim to examine and quantify the impact of fire aerosols on the
108 visibility and air quality of Southeast Asia over the past decade. Analyses of
109 observational data and comprehensive regional model results have both been performed
110 in order to improve our understanding of this issue. We firstly describe methodologies
111 adopted in the study, followed by the results and findings from our assessment of the fire
112 aerosol on the degradation of visibility in several selected cities and also over the whole
113 Southeast Asia. We then discuss the sensitivity of our findings to the use of different
114 meteorological datasets as well as fire emission inventories. The last section summarizes
115 and concludes our work.

116 **2 Methodology**

117 **2.1 The model**

118 In this study, we have used the Weather Research and Forecasting (WRF) model
119 coupled with a chemistry component (WRF-Chem) version 3.6 (Grell et al., 2005). Our
120 focus in this study is on the fire aerosol life cycle. Therefore, we chose to use WRF-
121 Chem with a modified chemical tracer module instead of a full chemistry package to thus
122 model the fire $PM_{2.5}$ particles as tracers without involving much more complicated

123 gaseous and aqueous chemical processing calculations but including dry and wet
124 depositions. Emissions of other chemical species were excluded in the simulations. This
125 configuration lowers the computational burden substantially, and thus allows us to
126 conduct long model integrations to determine the contributions of fire aerosol to the
127 degradation of visibility in the region over the past decade. In WRF-Chem, the sinks of
128 $PM_{2.5}$ particles include dry deposition and wet scavenging calculated at every time step.
129 The simulations are employed within a model domain with a horizontal resolution of 36
130 km, including 432×148 horizontal grid points (Fig. 1), and 31 vertically staggered layers
131 that are stretched to have a higher resolution near the surface (an average depth of ~ 30 m
132 in the first model half layer) based on a terrain-following pressure coordinate system.
133 The time step is 180 seconds for advection and physics calculation. The physics schemes
134 adopted in the simulations are listed in Table 1. The initial and boundary meteorological
135 conditions are taken from reanalysis meteorological data. In order to examine the
136 potential influence of different reanalysis products on simulation results, we have used
137 two such datasets: (1) the National Center for Environment Prediction FiNaL (NCEP-
138 FNL) reanalysis data (National Centers for Environmental Prediction, 2000), which has a
139 spatial resolution of 1 degree and a temporal resolution of 6 hours; and (2) ERA-Interim,
140 which is a global atmospheric reanalysis from the European Centre for Medium-Range
141 Weather Forecasts (ECMWF) (European Centre for Medium-Range Weather, 2009),
142 providing 6-hourly atmospheric fields on sixty pressure levels from surface to 0.1 hPa
143 with a horizontal resolution of approximately 80 km. Sea surface temperature is updated
144 every 6 hours in both NCEP-FNL and ERA-Interim. All simulations used four-
145 dimensional data assimilation (FDDA) to nudge NCEP-FNL or ERA-Interim

146 temperature, water vapor, and zonal as well as meridional wind speeds above the
147 planetary boundary layer (PBL). This approach has been shown to provide realistic
148 temperature, moisture, and wind fields in a long simulation (Stauffer and Seaman, 1994).

149 Two biomass burning emission inventories are also used in this study to investigate
150 the sensitivity of modeled fire aerosol concentration to different emission estimates. The
151 first emission inventory is the Fire INventory from NCAR version 1.5 (FINNv1.5)
152 (Wiedinmyer et al., 2011), which classifies burnings of extra tropical forest, tropical
153 forest (including peatland), savanna, and grassland. It is used in this study to provide
154 daily, 36 km resolution $PM_{2.5}$ emissions. The second emission inventory is the Global
155 Fire Emission Database version 4.1 with small fires included (GFEDv4.1s) (van der Werf
156 et al., 2010; Randerson et al., 2012; Giglio et al., 2013). GFEDv4.1s provides $PM_{2.5}$
157 emissions with the same spatiotemporal resolution as FINNv1.5.

158 Our simulations cover a time period slightly longer than a decade from 2003 to 2014
159 based on available biomass burning emission estimates. The simulation of each year
160 started on 1 November of the previous year and lasted for 14 months. The first two
161 months were used for spin-up.

162 Three sets of decadal long simulations have been conducted. The first simulation
163 used NCEP-FNL reanalysis data and the FINNv1.5 fire emission inventory. This
164 simulation is hereafter referred to as FNL_FINN and is discussed as the base simulation.
165 In order to examine the influence of different meteorological inputs on fire aerosol life
166 cycle, the second simulation was conducted using the same FINNv1.5 fire emission
167 inventory as in FNL_FINN but different reanalysis dataset, the ERA-Interim, and is
168 referred to as ERA_FINN. In addition, to investigate the variability of fire aerosol

169 concentration brought by the use of different estimates of fire emissions, the third
170 simulation, FNL_GFED, was driven by the same NCEP-FNL meteorological input as in
171 FNL_FINN but with a different fire emission inventory, the GFEDv4.1s.

172 A plume rise algorithm for fire emissions was implemented in WRF-Chem by Grell
173 et al. (2011) to estimate fire injection height. This algorithm, however, often derives an
174 injection height for tropical peat fire that is too high compared to the estimated value
175 based on remote sensing retrievals (Tosca et al., 2011). Therefore, we have limited the
176 plume injection height of peat fire by a ceiling of 700 m above the ground in this study
177 based on Tosca et al. (2011). The vertical distribution of emitted aerosols is calculated
178 using the plume model. This modification has clearly improved the modeled surface
179 PM_{2.5} concentration when compared to observations in Singapore.

180 In order to distinguish the spatial-temporal coverage and influence of biomass
181 burning aerosols from different regions in Southeast Asia and nearby northern Australia,
182 we have created five tracers to represent fire aerosols respectively from mainland
183 Southeast Asia (s1), Sumatra and Java islands (s2), Borneo (s3), the rest of the Maritime
184 Continent (s4), and northern Australia (s5) as illustrated in Fig. 1. Based on this design,
185 we are able to identify fire PM_{2.5} concentration from different regions and estimate the
186 contribution to the total fire PM_{2.5} in a receptor city.

187 Generally speaking, the major fire season in mainland Southeast Asia (s1) is from
188 February to April and in the other four regions (s2-s5), it is from August to October.
189 There is a strong anti-correlation between the seasonal variation of fire emissions and that
190 of rainfall in all fire regions as shown in Fig. 2. Because mainland Southeast Asia (s1)
191 and northern Australia (s5) are on the edge of the seasonal migration of the ITCZ, the

192 correlation in these two regions is even more pronounced. On the other hand, Sumatra
193 (s2), Borneo (s3) and the rest of the Maritime Continent (s4) do not have clearly
194 identifiable dry seasons and this contributes to the weaker correlation (Fig. 2b – d).
195 Besides that, underground peatland burning may not be immediately extinguished by
196 precipitation.

197 **2.2 Observational data and model derivation of visibility**

198 The definition of “visibility” is the farthest distance at which one can see a large,
199 black object against a bright background at the horizon (Seinfeld and Pandis, 2006).
200 There are several factors determining visibility, but here we mainly consider the
201 absorption and scattering of light by gases and aerosol particles, excluding fog or misty
202 days. In this study, the modeled visibility is calculated by using the *Koschmeider*
203 *equation*:

$$204 \quad \quad \quad VIS = 3.912 / b_{ext}, \quad (1)$$

205 where *VIS* is visibility with a unit in meter and b_{ext} is the extinction coefficient with a unit
206 of m^{-1} . Excluding fog, visibility degradation is most readily observed from the impact of
207 particulate pollution. Based on Eq. (1), a maximum visibility under an absolutely dry and
208 pollution-free air is about 296 km owing to Rayleigh scattering, while a visibility in the
209 order of 10 km is considered indicative of moderate to heavy air pollution by particulate
210 matter (Visscher, 2013). Abnormal and persistent low visibility situations are also
211 referred to as “haze” events. Air pollution sources such as fossil fuel burning, can cause
212 low visibility and haze events to occur. Similarly, fire aerosols, alone or mixed with
213 other particulate pollutants, can degrade visibility by increasing b_{ext} and lead to
214 occurrence of haze events too.

215 The observational data of visibility from the Global Surface Summary of the Day
216 (GSOD) (Smith et al., 2011) are used in our study to identify days under particulate
217 pollution, i.e., haze events. The GSOD is derived from the Integrated Surface Hourly
218 (ISH) dataset and archived at the National Climatic Data Center (NCDC). The daily
219 visibility in the dataset is available from 1973 to the present.

220 The observed visibility is also used to evaluate the modeled visibility and thus $PM_{2.5}$
221 concentration. The modeled visibility is derived based on the extinction coefficient of the
222 fire aerosols as a function of particle size, by assuming a log-normal size distribution of
223 accumulation mode with a standard deviation $\sigma = 2$ (Kim et al., 2008). Note that all
224 these calculations are done for the wavelength of 550 nm unless otherwise indicated. As
225 fire plumes contain both sulfur compounds and carbonaceous aerosols, we assume the
226 fire aerosols are aged internal mixtures with black carbon as the core and sulfate as the
227 shell (Kim et al., 2008). To make the calculated visibility of the fire aerosols better
228 match the reality, we have also considered hygroscopic growth of sulfate fraction of these
229 mixed particles in the calculation based on the modeled relative humidity (RH). Based
230 on Kiehl et al. (2000), the hygroscopic growth factor (rhf) is given by

$$231 \quad rhf = 1.0 + \exp \left(a_1 + \frac{a_2}{RH+a_3} + \frac{a_4}{RH+a_5} \right), \quad (2)$$

232 where a_1 to a_5 are fitting coefficients given by 0.5532, -0.1034, -1.05, -1.957, 0.3406,
233 respectively. The radius increase of wet particle (r_{wet}) due to hygroscopic growth will be

$$234 \quad r_{wet} = r_{dry}^{rhf}, \quad (3)$$

235 where r_{dry} is the radius of dry particle in micron.

236 As mentioned above, a visibility of 10 km is considered an indicator of moderate to
237 heavy particulate pollution. Hence an observed visibility of 10km is used as the

238 threshold for defining the “low visibility day (VLD)” in our study. We firstly derived the
239 observed low visibility days in every year for a given city using the GSOD visibility data.
240 Then, we derived the modeled low visibility days following the same procedure but using
241 modeled visibility data that were only influenced by fire aerosols. Both the observed and
242 modeled visibilities were then used to define the fraction of low visibility days that can
243 be explained by fire aerosols alone. It is assumed that whenever fire aerosol *alone* could
244 cause a low visibility day to occur, such a day would be attributed to fire aerosol caused
245 LVD, regardless of whether other coexisting pollutants would have a sufficient intensity
246 to cause low visibility or not. In addition to the LVD, we have also used a daily visibility
247 of 7 km as the criterion to define the observed “very low visibility day (VLVD)”. Such
248 heavy haze events in the region are generally caused by severe fire aerosol pollution, thus
249 we use their occurrence specifically to evaluate the model performance.

250 2.3 The “Haze Exposure Day (HED)”

251 We have derived a metric, the Haze Exposure Day (HED), to measure the exposure
252 of the whole Southeast Asia, represented by 50 cities of the Association of Southeast
253 Asian Nations (ASEAN), to low visibility events. HED can be defined in a population
254 weighted format for the analyzed 50 cities, indicating the relative exposure of the
255 populations in these cities to the low visibility events caused by particulate pollution:

$$256 \quad HED_{pw} = \sum_{i=1}^N C_{pw}(i), \quad (4)$$

257 where,

$$258 \quad C_{pw}(i) = pop(i) \cdot C(i) / \sum_{i=1}^N pop(i), \quad (5)$$

259 is the population-weighted fraction of the total Haze Exposure Days, N equals to the total
260 number of cities (50), i is the index for the 50 analyzed cities, $pop(i)$ is the population for

261 a given city (Table S1), and $C(i)$ represents the annual LVDs for that city calculated from
262 the GSOD dataset. Note that we assume that the population of each city stays constant
263 throughout the analyzed period. Another assumption of HED_{pw} is that everyone in a
264 given city would be equally exposed to the particulate pollution.

265 In addition, HED can be also defined in an arithmetic mean format, assuming each
266 city weights equally regardless of its population. Its value hence emphasizes on the
267 relative exposure of each area within the analyzed region:

$$268 \quad HED_{ar} = \sum_{i=1}^N C(i)/N. \quad (6)$$

269 Both HED_{pw} and HED_{ar} can be also calculated using fire-caused LVDs to define the
270 absolute and relative contributions of fire aerosols to the total low visibility events in the
271 region. We will label the fire-caused HED as $fHED_{pw}$ and $fHED_{ar}$.

272 **3 Assessment of the impact of fire aerosols on the visibility in Southeast Asia**

273 **3.1 Impact of fire aerosols on the visibility in four selected cities**

274 We first to focus our analysis on four selected cities in the region, Bangkok
275 (Thailand), Kuala Lumpur (Malaysia), Singapore (Singapore), and Kuching (Malaysia),
276 all located close to the major fire sites ranging from the mainland to the islands of
277 Southeast Asia. Specifically, Bangkok is a smoke receptor city for the fire events in
278 mainland of Southeast Asia (s1) while Kuala Lumpur and Singapore are two cities
279 frequently under the influence of Sumatra (s2) as well as Borneo fires (s3). Kuching is in
280 the coastal area of Borneo and directly affected by Borneo fire events (s3).

281 The surface observational data of $PM_{2.5}$ concentration among these four cities are
282 only available in Singapore since 2013 from the National Environment Agency (NEA) of

283 Singapore. We thus firstly used these data along with visibility data to evaluate the
284 model's performance for fire-caused haze events reported in Singapore during 2013-2014
285 (Fig. 3). Note that the observed $PM_{2.5}$ level reflects the influences of both fire and non-
286 fire aerosols, whereas the modeled $PM_{2.5}$ only includes the impact of fire aerosols. We
287 find that the model still predicted clearly high $PM_{2.5}$ concentrations during most of the
288 observed haze events, especially in June 2013, and in spring and fall seasons of 2014,
289 though with underestimates in particle concentration of up to 30-50%, likely due to the
290 model's exclusion of non-fire aerosols, coarse model resolution, overestimated rainfall,
291 or errors in the emission inventory. Figure 4 shows observed visibility versus modeled
292 visibility in FNL_FINN during the fire events shown in Fig. 3. Note that all these events
293 have an observed visibility lower than or equal to 10 km, or can be identified as LVDs.
294 In capturing these fire-caused haze events, the model only missed about 22% of them,
295 reporting a visibility larger than 10 km in 40 out of 185 observed LVDs as marked with
296 purple color in Fig. 4. When observed visibility is between 7 and 10 km, model results
297 appear to align with observations rather well. For cases with visibility lower than 7 km,
298 the model captured all the events (by reporting a visibility lower than 10 km, or LVD)
299 although often overestimated the visibility range. These results imply that the VLVDs
300 only count a very small fraction in LVDs and thus are episodic events. It is very likely
301 that the size of concentrated fire plumes in VLVDs might be constantly smaller than the
302 36 km model resolution; therefore, the model results could not reach the peak values of
303 $PM_{2.5}$ concentrations of these plumes.

304 Furthermore, the LVDs in the four selected near-fire-site cities during the fire
305 seasons from 2003 to 2014 have been identified using the daily GSOD visibility database

306 and then compared with modeled results (Fig. 5). It is difficult to identify all the fire
307 caused haze events beyond Singapore even in recent years. However, in Southeast Asia,
308 severe haze events equivalent to the VLVDs in visibility degradation are known to be
309 largely caused by fire aerosol pollution. Therefore, we used the observed VLVDs in the
310 four selected cities to evaluate the performance of the model. We find that the modeled
311 result displays a good performance in capturing VLVDs despite an overestimate in
312 visibility range during certain events compared with the observation. The model in
313 general only missed about 10% or fewer VLVDs observed in the past decade (Table 2;
314 Fig. 5). In addition, the model has reasonably captured the observed LVDs despite
315 certain biases (Fig. 5), likely due to the fact that fire aerosol might not be the only reason
316 responsible for the degradation of visibility during many LVDs.

317 We find that the annual mean LVDs in Bangkok has increased from 47% (172 days)
318 in the first 5-year period of the simulation duration (2003-2007) to 74% (272 days) in the
319 last 5-year period (2010-2014). The LVDs caused by fire aerosols has increased as well
320 (Fig. 6a). Overall, fire aerosols are responsible for more than one third of these LVDs
321 (i.e., 39% in average; Table 2). The largest source of fire aerosols affecting Bangkok is
322 burning of agriculture waste and other biomass in s1 during the dry season of spring (Fig.
323 7a; Table 3). During the fire season, abundant fire aerosols degrade visibility and even
324 cause VLVDs to occur, mainly from December to April (Fig. 6e). Based on our model
325 results, 87% of VLVDs can be identified as caused by fires.

326 In Kuala Lumpur, the percentage of LVDs also gradually increases since 2006 to
327 reach a peak in 2011 and again in 2014 (Fig. 6b). During 2005-2010 the frequency of
328 total LVDs have increased 10-15% each year, mainly attributing to the pollution sources

329 other than fires. However, fire-caused LVDs become more evident after 2009. Seasonal
330 wise, there are two peaks of fire aerosol influence, one in February-March and another in
331 August (Fig. 6f), corresponding to the trans-boundary transport of fire aerosols from
332 mainland Southeast Asia (s1) in the winter monsoon season and from Sumatra (s2) in the
333 summer monsoon season, respectively (Fig. 7b). Three quarter of VLVDs occurred in
334 the summer monsoon season due to Sumatra fires. Note that in November and December
335 the percentage of LVDs is over 50% and dominated by pollutants other than fire aerosols.
336 These non-fire aerosols presumably come from either local sources or the areas further
337 inland riding on the winter monsoon circulation. Overall, fire pollution is responsible for
338 36%, a substantial fraction of total low visibility events in Kuala Lumpur during 2003-
339 2014 (Table 2).

340 The percentage of LVDs in Singapore has been rapidly increasing since 2012 (Fig.
341 6c). During the simulation period, this increase appears to be mostly from anthropogenic
342 pollution other than fires, especially in 2012 and 2013. In monthly variation, similarly to
343 Kuala Lumpur, two peaks of fire aerosol influence appear in February-March and in
344 September-October, respectively (Fig. 6g). In February and March, the trans-boundary
345 transport of fire aerosols come from mainland Southeast Asia (s1), while in the summer
346 monsoon season fire aerosols come from both Sumatra (s2) and Borneo (s3) (Fig. 7c).
347 Except for the severe haze events in June 2013, VLVDs basically occur in September and
348 October (i.e., 92%) due to both Sumatra and Borneo fires. In general, up to 34% of
349 LVDs in Singapore are caused by fire aerosols based on the FNL_FINN simulation and
350 the rest by local and long-range transported pollutants (Table 2). Nevertheless, fire
351 aerosol is still the major reason for the episodic severe haze conditions.

352 Because of its geographic location, Kuching is affected heavily by local fire events
353 during the fire season (Fig. 7d). Fire aerosols can often degrade the visibility to below 7
354 km and even reaching 2 km (Fig. 5d). The LVDs mainly occur in August and September
355 during the fire season (Fig. 6d and h). The frequency of LVDs in Kuching is similarly to
356 Singapore; however, 25% of those LVDs are considered to be VLVDs in Kuching while
357 only 4% are in Singapore in comparison (Table 2).

358 **3.2 Impact of fire aerosols on the visibility over the whole Southeast Asia**

359 Air quality degradation caused by fires apparently occurs in regions beyond the
360 above-analyzed four cities. To examine such degradation over the whole Southeast Asia,
361 we have extended our analysis to cover 50 cities of the ASEAN. The impact of
362 particulate pollution on the whole Southeast Asia is measured by the “Haze Exposure
363 Day” (HED) as defined in Section 2.3. The top four among the 50 cities that made the
364 largest contributions to the HED_{pw} are Jakarta, Bangkok, Hanoi, and Yangon (Fig. 8a),
365 with population ranking of 1, 2, 4, and 5, respectively (Table S1).

366 We find that both HED_{pw} and HED_{ar} increase rather steadily over the past decade
367 (Fig. 8b), demonstrating that the exposure to haze events either weighted by population
368 or not has become worse in the region. Generally speaking, the fire aerosols are
369 responsible for up to 40-60% of the total exposure to low visibility across the region. In
370 both measures, the increase of fire-caused HED (2.64 and 3.37 days per year for
371 population-weighted and arithmetic mean, respectively) is similarly to that of overall
372 HED (2.61 and 3.59 days per year for population-weighted and arithmetic mean,
373 respectively) (Fig. 8b), suggesting that fire aerosol has taken the major role in degrading
374 air quality in Southeast Asia compared to the non-fire particulate pollution. The result

375 that HED_{pw} is higher than HED_{ar} in most of the years indicates that the particulate
376 pollution is on average worse over more populous cities than the others. Interestingly,
377 the discrepancy of these two variables, however, has become smaller in recent years and
378 even reversed in 2014, implying an increase of haze occurrence across cities with
379 different populations in the region. The reason behind this could be a wider spread of fire
380 events in the region, causing acute haze events in cities even with relatively low
381 populations. Regarding the increase of fire-caused HED, because biomass burning,
382 especially peatland burning, usually occurs in the rural areas, higher fire emissions would
383 extend low visibility conditions to a larger area regardless of its population. On the other
384 hand, due to industrialization, urbanization, and other factors such as population growth,
385 air pollution has become worse across the region so even cities with lower populations
386 now increasingly suffer from low visibility from fossil fuel burning and other sources of
387 particulate pollution (IEA, 2015). Therefore, the mitigation of air quality degradation
388 needs to consider both fire and non-fire sources.

389 **3.3 The influence of wind and precipitation on fire aerosol life cycle**

390 Seasonal migrations of the ITCZ and associated summer and winter monsoons
391 dominate seasonal wind flows that drive fire aerosol transport. Additionally, as discussed
392 previously, certain small-scale or short-term phenomena such as sea breezes, typhoons,
393 and topography-forced circulations also play important roles in distributing fire aerosols.
394 Nevertheless, we focus our discussion here on the former.

395 From February to April is the main fire season in mainland Southeast Asia (s1). In
396 the FNL_FINN simulation, the seasonal mean concentration of $PM_{2.5}$ within the PBL can
397 exceed $20 \mu g m^{-3}$ in this region (note that the air quality standard suggested by World

398 Health Origination is $10 \mu\text{g m}^{-3}$ for annual mean and $25 \mu\text{g m}^{-3}$ for 24-h mean). During
399 this fire season, the most common wind direction is from northeast to southwest across
400 the region (Fig. 9a). Fire aerosol plumes with concentrations higher than $0.1 \mu\text{g m}^{-3}$ can
401 be transported westward as far as 7000 km from the burning sites (Fig. 9a). In contrast,
402 February to April is not the typical burning season in the islands. Low fire emissions in
403 combination with a lack of long-range transport of fire aerosols from the mainland due to
404 the seasonal circulation result in a low $\text{PM}_{2.5}$ level over these regions (Fig. 9b - d).

405 Wet scavenging is a major factor determining the lifetime and thus abundance of
406 suspended fire aerosols in the air. The effect of wet scavenging of fire aerosols is
407 reflected from the wet scavenging time calculated using the modeled results, which is a
408 ratio of the aerosol mass concentration to the scavenging rate (a function of precipitation
409 rate). Thus, short scavenging times often indicate high scavenging rates except for the
410 sites with extremely low aerosol concentration. During February-April, at the ITCZ's
411 furthest southern extent, the short scavenging time < 1 day around 10°S shows a quick
412 removal of fire aerosols by heavy precipitation, preventing the southward transport of
413 aerosols (Fig. 9f). On the other hand, the long scavenging time (> 5 days) in the Western
414 Pacific warm pool, South China Sea, the Indochina peninsula, Bay of Bengal, and
415 Arabian Sea leads to a long suspending time of aerosols transported to these regions.
416 During the same season, over the islands of Sumatra and Borneo, the abundance of fire
417 aerosols, either emitted locally or trans-boundary transported, are greatly limited by the
418 high scavenging rate (short scavenging time) over these regions (Fig. 9g and h). The
419 South China Sea has little precipitation during this time period; therefore, fire aerosols

420 from the northern part of the Philippines can be transported to this region and stay longer
421 than 5 days (Fig. 9i).

422 The months of August to October, when the ITCZ reaches its furthest northern
423 extent, mark the major fire season of Sumatra, Borneo, and some other islands in the MC
424 (Fig. S1b - d). Australia fires also mainly occur in this season (Fig. S1e). Mean wind
425 flows are from southeast to northwest in the Southern Hemisphere, and turn to the
426 northeast direction once past the Equator. Within the MC the seasonal variation of
427 rainfall is small during this time, with heavy precipitation and thus short scavenging
428 times (< 3 days) existing along the MJO path (Fig. S1f - i) (Wu and Hsu, 2009). The
429 high scavenging rate in the regions close to the fire sites in the islands shortens the
430 transport distance of fire aerosol plumes with $PM_{2.5}$ concentration $> 0.1 \mu g m^{-3}$ to less
431 than 3000 km (Fig. S1b - d). Long scavenging times (> 5 days) exist in the Banda Sea
432 and northern Australia due to the ITCZ location. Fire aerosols from Java (s2) (Fig. S1g),
433 Papua New Guinea (s4) (Fig. S1i), and northern Australia (s5) (Fig. S1j) can thus be
434 suspended in the air for a relatively long time over these regions.

435 The above-discussed seasonal features of precipitation and aerosol scavenging
436 rate help us to better understand the variability of haze occurrence and also to
437 identify the major source regions of fire aerosols influencing selected Southeast
438 Asian cities (Fig. 7). For example, the geographic location of Bangkok, which is
439 inside the s1 emission region, determines that nearly all the fire aerosols (99%) are
440 from sources within the region from December to April (Fig. 7a and Table 3). Fire
441 aerosols from all the other burning sites stay at very low levels even during the
442 burning seasons there due to circulation and precipitation scavenging. For Kuala

443 Lumpur and Singapore, over 90% of the fire aerosols reaching both cities come from
444 mainland Southeast Asia (s1) in January–April due to the dominant winter monsoon
445 circulation. During May–October, however, the major sources of fire aerosols shift to
446 Sumatra (s2) and Borneo (s3) aided by northward wind (Fig. S1b and c). The
447 monthly variations of PM_{2.5} concentration in Kuala Lumpur and Singapore also have
448 a largely similar pattern (Fig. 7b and c). The annual mean contribution of different
449 emission regions in Kuala Lumpur are 43% from mainland Southeast Asia (s1), 50%
450 from Sumatra (s2), 4% from Borneo (s3), 3% from the rest of Maritime Continent
451 (s4), and 0.3% from northern Australia (s5) in FINL_FINN (Table 3). Similarly to
452 Kuala Lumpur, there are two peak seasons of the monthly low visibility days
453 contributed by fire aerosols in Singapore (Fig. 6g), well correlated with modeled
454 high fire PM_{2.5} concentration (Fig. 7c). The low visibility days in March and April
455 mainly are caused by fire aerosols from mainland Southeast Asia (s1) under
456 southward wind pattern (Fig. 9a), and those in May to October are affected by
457 Sumatra (s2) first in May to June, and then by both s2 and s3 (Borneo) during
458 August to October due to north- or northwest-ward monsoonal circulation (Fig. S1b
459 and c; also Table 3). Kuching, similarly to Bangkok, is strongly affected by local fire
460 aerosols (s3) during the fire season (July – October). The annual mean contribution
461 from Borneo (s3) is 85%, with only 8% from mainland Southeast Asia (s1) and 5%
462 | from Sumatra (s2) (Table 3).

463 **4 Influence of different meteorological datasets and emission inventories on**
464 **modeled fire aerosol abundance**

465 **4.1 Different meteorological datasets**

466 Meteorological conditions, particularly wind fields and precipitation, could
467 substantially influence the life cycle and transport path of fire aerosols during the fire
468 seasons. First of all, we use these two variables to evaluate the model's performance in
469 simulating meteorological features. The WRF simulation driven by NCEP-FNL
470 reanalysis data, the FNL_FINN run, produced a monthly mean precipitation of 6.80 ± 0.55
471 mm day^{-1} over the modeled domain for the period from 2003 to 2014, very close to the
472 value of $6.30 \pm 0.43 \text{ mm day}^{-1}$ produced in another simulation driven by ERA-Interim, the
473 ERA_FINN run. However, the average rainfall in both runs appears to be higher than the
474 monthly mean of $4.71 \pm 0.37 \text{ mm day}^{-1}$ from the satellite-retrieved precipitation of the
475 Tropical Rainfall Measuring Mission (TRMM) 3B43 (V7) dataset (Huffman et al., 2007).
476 Based on the sensitivity tests for FDDA grid nudging, the wet bias in both experiments
477 mainly comes from water vapor nudging. Figure S2a – c are the Hovmöller plots of daily
478 TRMM, FNL_FINN, and ERA_FINN precipitation in 2006, respectively. Compared to
479 the satellite-retrieved data, both FNL_FINN and ERA_FINN have produced more light
480 rain events, and this appears to be the reason behind the model precipitation bias.
481 Despite the model overestimate in average total precipitation, the temporal correlation of
482 monthly rainfall between FNL_FINN and TRMM is 0.68 and the spatial correlation is
483 0.85 during 2003-2014 (Table 2). For ERA_FINN, the temporal correlation with TRMM
484 is 0.90, while the spatial correlation is 0.85. In the summer monsoon season (i.e., May,
485 June and July), both runs show the highest temporal correlations with observation but the

486 lowest in the spatial correlations. The comparisons show that simulated rainfall generally
487 agrees with the observation in space and time, especially when ERA-Interim reanalysis is
488 used (i.e., in ERA_FINN).

489 The representative wind pattern in Southeast Asia is the monsoon wind flow. In the
490 winter monsoon season (i.e., February, March and April), mean surface winds are from
491 northeast in the Northern Hemisphere and turn to the northwesterly once past the Equator
492 (Fig. S3a). On the other hand, the wind directions are reversed in the summer monsoon
493 season (i.e., August, September and October) (Fig. S3b). We use the wind data from
494 NCEP-FNL and ERA-Interim reanalysis to evaluate model simulated winds. We find
495 that both runs overestimated the u component (stronger easterly) in South China Sea (Fig.
496 S4a and c) in the winter monsoon season, and overestimated the v component (stronger
497 southerly) in Java Sea in the summer monsoon season (Fig. S4b and d). These regions
498 are the entrances of monsoon wind flow into the MC. In general, the model has well
499 captured the general wind flows in Southeast Asia during both monsoon seasons but
500 overestimated about 1 m s^{-1} in wind speed in some regions likely due to terrain effect and
501 model resolution limitation.

502 When comparing two of our simulations, FNL_FINN and ERA_FINN, we find that
503 the ERA_FINN run consistently produces less precipitation than the FNL_FINN run
504 during the rainy seasons over the past decade (Fig. 2). Regarding fire aerosol life cycle,
505 less rainfall in ERA_FINN results in weaker wet scavenging and thus higher abundance
506 of fire aerosols than in FNL_FINN. We find that the annual mean concentration of fire
507 $\text{PM}_{2.5}$ produced in the ERA_FINN run in Bangkok, Kuala Lumpur, Singapore, and
508 Kuching is 9.2, 5.8, 3.4, and $7.7 \mu\text{g m}^{-3}$, respectively, clearly higher than the

509 corresponding results of the FNL_FINN run of 8.5, 5.3, 3.0, and 6.9 $\mu\text{g m}^{-3}$ (Table 3). In
510 general, fire $\text{PM}_{2.5}$ concentration in ERA_FINN is about 10% higher than in FNL_FINN.
511 However, the occurrence of low visibility events is less sensitive to the differences in
512 rainfall in places near the burning areas such as Bangkok and Kuching, as indicated by a
513 nearly negligible enhancement of VLVDs in the ERA_FINN run in Bangkok and
514 Kuching (~1%) (Table 2). In comparison, the difference in wind fields between the two
515 runs has a much smaller impact than that of precipitation on modeled particulate matter
516 abundance.

517 **4.2 Different biomass burning emission inventories**

518 In addition to meteorological inputs, using different fire emission estimates could
519 also affect the modeled $\text{PM}_{2.5}$ concentration. To examine this impact, we have compared
520 two simulations with the same meteorological input but different fire emission
521 inventories, the FNL_FINN using FINNv1.5 and FNL_GFED using GFEDv4.1s. The
522 main differences between the two emission inventories appear mostly in mainland
523 Southeast Asia (s1) and northern Australia (s5) (Fig. 2a and e). Compared to FINNv1.5,
524 fire emissions in GFEDv4.1s over mainland Southeast Asia are more than 66% lower
525 (Fig. 2a), and this results in a 43% lower fire $\text{PM}_{2.5}$ concentration in Bangkok (Table 3).
526 The lower fire $\text{PM}_{2.5}$ concentration in FNL_GFED actually produces a visibility that
527 matches better with observations in Bangkok comparing to the result of FNL_FINN (Fig.
528 S5a). This implies that the fire emissions in FINNv1.5 are perhaps overestimated in
529 mainland Southeast Asia. In northern Australia, fire aerosol emissions suggested by
530 FINNv1.5 are almost negligible compared to GFEDv4.1s (Fig. 2e). Therefore, in the
531 FNL_GFED simulation, Australia fire aerosols play an important role in Singapore air

532 quality, contributing to about 22% of the modeled $PM_{2.5}$ concentration in Singapore. In
533 contrast, Australia fires have nearly no effect on Singapore air quality in the FNL_FINN
534 run (Table 3).

535 We would also like to point out the importance of spatiotemporal distribution of fire
536 emission to the modeled $PM_{2.5}$ concentration. For example, during the June 2013 severe
537 haze event in Kuala Lumpur and Singapore, the total amount of fire emissions from
538 Sumatra (s2) in GFEDv4.1s are lower than those of FINNv1.5 (Fig. S6a) but distributed
539 rather more densely over a smaller area (Fig. S6c and d). As a result, under the same
540 meteorological conditions, the simulated $PM_{2.5}$ in the FNL_GFED simulation reaches
541 Singapore in a higher concentration that also matches better with observations than the
542 result of FNL_FINN (Fig. S6b).

543 Reddington et al. (2014) applied two different models, a 3D global chemical
544 transport model and a Lagrangian tracer model to examine the long-term mean
545 contributions of fire emissions from different regions to $PM_{2.5}$ in several cities in
546 Southeast Asia. Their estimated contribution from mainland Southeast Asia to the above-
547 discussed four selected cities in Section 3.1 was lower than our result during January-
548 May, likely due to their use of a different emission inventory and the coarse resolution of
549 their global model. The FINNv1.5 dataset used in our study specifically provides higher
550 $PM_{2.5}$ emissions from agriculture fires (the major fire type in mainland Southeast Asia)
551 than GFED4.1s does – the latter is an updated version of the dataset (GFEDv3) used in
552 Reddington et al. (2014) (Fig. 2).

553 **5 Summary and Conclusions**

554 We have examined the extent of the biomass burning aerosol's impact on the air
555 quality of Southeast Asia over the past decade using surface visibility and $PM_{2.5}$
556 measurements along with the WRF model with a modified fire tracer module. The model
557 has shown a good performance in capturing 90% of the observed severe haze events
558 (visibility < 7 km) caused by fire aerosols occurred over the past decade in several cities
559 that are close to the major burning sites. Our study also suggests that fire aerosols are
560 responsible for a substantial fraction of the low visibility days (visibility < 10 km) in
561 these cities: up to 39% in Bangkok, 36% in Kuala Lumpur, 34% in Singapore, and 33%
562 in Kuching.

563 In attributing the low visibility events to fire emissions from different sites, we find
564 that mainland Southeast Asia is the major contributor during the northeast or winter
565 monsoon season in Southeast Asia. In the southwest or summer monsoon season,
566 however, most fire aerosols come from Sumatra and Borneo. Specifically, fires in
567 mainland Southeast Asia account for the largest percentage of the total fire $PM_{2.5}$ in
568 Bangkok (99%), and fires from Sumatra are the major contributor in Kuala Lumpur
569 (50%) and Singapore (41%). Kuching receives 85% of fire aerosols from local Borneo
570 fires.

571 By comparing the results from two modeled runs with the same fire emissions but
572 driven by different meteorological inputs, we have examined the sensitivity of modeled
573 results to meteorological datasets. The discrepancy in modeled low visibility events
574 arising from the use of different meteorological datasets is clearly evident, especially in
575 the results of Bangkok and Kuching. However, using different meteorological input

576 datasets does not appear to have influenced the modeled very low visibility events, or the
577 severe haze events in the cities close to burning sites.

578 We have also examined the sensitivity of modeled results to the use of different
579 emission inventories. We find that significant discrepancies of fire emissions in
580 mainland Southeast Asia and northern Australia between the two emission inventories
581 used in our study have caused a substantial difference in modeled fire aerosol
582 concentration and visibility, especially in Bangkok and Singapore. For instance, the
583 contribution to fire aerosol in Singapore from northern Australia changes from nearly
584 zero in the simulation driven by FINNv1.5 to about 22% in another simulation driven by
585 GFEDv4.1s. Based on these results, we suggest further research is needed to improve the
586 current estimate of the spatiotemporal distribution of fire emissions, in addition to total
587 emitted quantities from the fire hotspots.

588 To further assess the impacts of particulate pollution on the surface visibility of the
589 whole Southeast Asia and to estimate the fire aerosol's contribution, we have defined and
590 derived a metric of "Haze Exposure Days" (HEDs), by integrating annual low visibility
591 days of 50 cities of the Association of Southeast Asian Nations and weighted by
592 population or averaged arithmetically. We find that a very large population of Southeast
593 Asia has been exposed to relatively persistent hazy conditions. The top four cities in the
594 HED ranking, Jakarta, Bangkok, Hanoi, and Yangon, with a total population exceeding
595 30 million, all have experienced more than 200 days per year of low visibility due to
596 particulate pollution over the past decade and more than 50% of those low visibility days
597 were mainly due to fire aerosols. Even worse is that the number of annual low visibility
598 days have been increasing steadily not only in high population cities but also those with

599 relatively low populations, suggesting widespread particulate pollution across Southeast
600 Asian. In summary, the fire aerosols are found to be responsible for up to about half of
601 the total exposures to low visibility in the region. This result suggests that in order to
602 improve the air quality in Southeast Asia, besides reducing or even prohibiting planned or
603 unplanned fires, mitigation policies targeting pollution sources other than fires also needs
604 to be implemented.

605

606 **Acknowledgements.**

607 This research was supported by the National Research Foundation Singapore through the
608 Singapore-MIT Alliance for Research and Technology, the interdisciplinary research
609 program of Center for Environmental Sensing and Modeling. It was also supported by
610 the U.S. National Science Foundation (AGS-1339264), U.S. DOE (DE-FG02-
611 94ER61937) and U.S. EPA (XA-83600001-1). The authors would like to acknowledge
612 the National Environment Agency (NEA) of Singapore for making Singapore PM_{2.5} data
613 available; the NCEP-FNL, ECMWF ERA-Interim, NCAR FINN, and GFED working
614 groups for releasing their data to the research communities; and the NCAR WRF
615 developing team for providing the numerical model for this study. We thank the National
616 Supercomputing Centre of Singapore (NSCC) for providing computing resources and
617 technical support. Two anonymous reviewers provided many constructive suggestions
618 and comments, leading to a substantial improvement of the manuscript.

619

620 **Reference**

621 Carlson, K. M., Curran, L. M., Ratnasari, D., Pittman, A. M., Soares-Filho, B. S., Asner, G.
622 P., Trigg, S. N., Gaveau, D. A., Lawrence, D., and Rodrigues, H. O.: Committed

623 carbon emissions, deforestation, and community land conversion from oil
624 palm plantation expansion in West Kalimantan, Indonesia, *Proceedings of the*
625 *National Academy of Sciences*, 109, 7559-7564, 10.1073/pnas.1200452109,
626 2012.

627 Chang, C. P., Wang, Z., McBride, J., and Liu, C.-H.: Annual Cycle of Southeast Asia—
628 Maritime Continent Rainfall and the Asymmetric Monsoon Transition,
629 *Journal of Climate*, 18, 287-301, 10.1175/JCLI-3257.1, 2005.

630 Crippa, P., Castruccio, S., Archer-Nicholls, S., Lebron, G. B., Kuwata, M., Thota, A.,
631 Sumin, S., Butt, E., Wiedinmyer, C., and Spracklen, D. V.: Population exposure
632 to hazardous air quality due to the 2015 fires in Equatorial Asia, *Scientific*
633 *Reports*, 6, 37074, 10.1038/srep37074, 2016.

634 Dennis, R., Mayer, J., Applegate, G., Chokkalingam, U., Colfer, C. P., Kurniawan, I.,
635 Lachowski, H., Maus, P., Permana, R., Ruchiat, Y., Stolle, F., Suyanto, and
636 Tomich, T.: Fire, People and Pixels: Linking Social Science and Remote
637 Sensing to Understand Underlying Causes and Impacts of Fires in Indonesia,
638 *Hum Ecol*, 33, 465-504, 10.1007/s10745-005-5156-z, 2005.

639 Emmanuel, S. C.: Impact to lung health of haze from forest fires: The Singapore
640 experience, *Respirology*, 5, 175-182, 10.1046/j.1440-1843.2000.00247.x,
641 2000.

642 European Centre for Medium-Range Weather, F.: ERA-Interim Project,
643 10.5065/D6CR5RD9, 2009.

644 Field, R. D., van der Werf, G. R., and Shen, S. S. P.: Human amplification of drought-
645 induced biomass burning in Indonesia since 1960, *Nature Geosci*, 2, 185-188,
646 http://www.nature.com/ngeo/journal/v2/n3/supinfo/ngeo443_S1.html,
647 2009.

648 Fujii, Y., Iriana, W., Oda, M., Puriwigati, A., Tohno, S., Lestari, P., Mizohata, A., and
649 Huboyo, H. S.: Characteristics of carbonaceous aerosols emitted from
650 peatland fire in Riau, Sumatra, Indonesia, *Atmospheric Environment*, 87,
651 164-169, <http://dx.doi.org/10.1016/j.atmosenv.2014.01.037>, 2014.

652 Giglio, L., Randerson, J. T., and van der Werf, G. R.: Analysis of daily, monthly, and
653 annual burned area using the fourth-generation global fire emissions
654 database (GFED4), *Journal of Geophysical Research: Biogeosciences*, 118,
655 317-328, 10.1002/jgrg.20042, 2013.

656 Grandey, B. S., Lee, H. H., and Wang, C.: Radiative effects of interannually varying vs.
657 interannually invariant aerosol emissions from fires, *Atmos. Chem. Phys.*, 16,
658 14495-14513, 10.5194/acp-16-14495-2016, 2016.

659 Grell, G., Freitas, S. R., Stuefer, M., and Fast, J.: Inclusion of biomass burning in WRF-
660 Chem: impact of wildfires on weather forecasts, *Atmos. Chem. Phys.*, 11,
661 5289-5303, 10.5194/acp-11-5289-2011, 2011.

662 Grell, G. A., Peckham, S. E., Schmitz, R., McKeen, S. A., Frost, G., Skamarock, W. C., and
663 Eder, B.: Fully coupled “online” chemistry within the WRF model,
664 *Atmospheric Environment*, 39, 10.1016/j.atmosenv.2005.04.027, 2005.

665 Heil, A., Langmann, B., and Aldrian, E.: Indonesian peat and vegetation fire
666 emissions: Study on factors influencing large-scale smoke haze pollution
667 using a regional atmospheric chemistry model, *Mitig Adapt Strat Glob*
668 *Change*, 12, 113-133, 10.1007/s11027-006-9045-6, 2007.

669 Huffman, G. J., Bolvin, D. T., Nelkin, E. J., Wolff, D. B., Adler, R. F., Gu, G., Hong, Y.,
670 Bowman, K. P., and Stocker, E. F.: The TRMM Multisatellite Precipitation
671 Analysis (TMPA): Quasi-Global, Multiyear, Combined-Sensor Precipitation
672 Estimates at Fine Scales, *Journal of Hydrometeorology*, 8, 38-55,
673 10.1175/JHM560.1, 2007.

674 IEA: Energy and Climate Change, World Energy Outlook Special Report,
675 International Energy Agency, pp. 74 -77, 2015.

676 Johnston, F. H., Henderson, S. B., Chen, Y., Randerson, J. T., Marlier, M., Defries, R. S.,
677 Kinney, P., Bowman, D. M., and Brauer, M.: Estimated global mortality
678 attributable to smoke from landscape fires *Environ. Health Perspect.* , 120
679 695–701, 2012.

680 Kiehl, J. T., Schneider, T. L., Rasch, P. J., Barth, M. C., and Wong, J.: Radiative forcing
681 due to sulfate aerosols from simulations with the National Center for
682 Atmospheric Research Community Climate Model, Version 3, *Journal of*
683 *Geophysical Research: Atmospheres*, 105, 1441-1457,
684 10.1029/1999JD900495, 2000.

685 Kim, D., Wang, C., Ekman, A. M. L., Barth, M. C., and Rasch, P. J.: Distribution and
686 direct radiative forcing of carbonaceous and sulfate aerosols in an interactive
687 size-resolving aerosol–climate model, *Journal of Geophysical Research:*
688 *Atmospheres*, 113, D16309, 10.1029/2007jd009756, 2008.

689 Koe, L. C. C., Arellano Jr, A. F., and McGregor, J. L.: Investigating the haze transport
690 from 1997 biomass burning in Southeast Asia: its impact upon Singapore,
691 *Atmospheric Environment*, 35, 2723-2734,
692 [http://dx.doi.org/10.1016/S1352-2310\(00\)00395-2](http://dx.doi.org/10.1016/S1352-2310(00)00395-2), 2001.

693 Kunii, O., Kanagawa, S., Yajima, I., Hisamatsu, Y., Yamamura, S., Amagai, T., and
694 Ismail, I. T. S.: The 1997 Haze Disaster in Indonesia: Its Air Quality and Health
695 Effects, *Archives of Environmental Health: An International Journal*, 57, 16-
696 22, 10.1080/00039890209602912, 2002.

697 Langner, A., Miettinen, J., and Siegert, F.: Land cover change 2002–2005 in Borneo
698 and the role of fire derived from MODIS imagery, *Global Change Biology*, 13,
699 2329-2340, 10.1111/j.1365-2486.2007.01442.x, 2007.

700 Lin, N.-H., Tsay, S.-C., Maring, H. B., Yen, M.-C., Sheu, G.-R., Wang, S.-H., Chi, K. H.,
701 Chuang, M.-T., Ou-Yang, C.-F., Fu, J. S., Reid, J. S., Lee, C.-T., Wang, L.-C., Wang,
702 J.-L., Hsu, C. N., Sayer, A. M., Holben, B. N., Chu, Y.-C., Nguyen, X. A., Sopajaree,
703 K., Chen, S.-J., Cheng, M.-T., Tsuang, B.-J., Tsai, C.-J., Peng, C.-M., Schnell, R. C.,
704 Conway, T., Chang, C.-T., Lin, K.-S., Tsai, Y. I., Lee, W.-J., Chang, S.-C., Liu, J.-J.,
705 Chiang, W.-L., Huang, S.-J., Lin, T.-H., and Liu, G.-R.: An overview of regional
706 experiments on biomass burning aerosols and related pollutants in Southeast
707 Asia: From BASE-ASIA and the Dongsha Experiment to 7-SEAS, *Atmospheric*
708 *Environment*, 78, 1-19, <http://dx.doi.org/10.1016/j.atmosenv.2013.04.066>,
709 2013.

710 Madden, R. A., and Julian, P. R.: Detection of a 40–50 Day Oscillation in the Zonal
711 Wind in the Tropical Pacific, *Journal of the Atmospheric Sciences*, 28, 702-
712 708, 10.1175/1520-0469(1971)028<0702:DOADOI>2.0.CO;2, 1971.

713 Marlier, M., Defries, R. S., Kim, P. S., Koplitz, S. N., Jacob, D. J., Mickley, L. J., and Myers,
714 S. S.: Fire emissions and regional air quality impacts from fires in oil palm,

715 timber, and logging concessions in Indonesia, *Environmental Research*
716 *Letters*, 10, 085005, 2015a.

717 Marlier, M. E., DeFries, R. S., Kim, P. S., Gaveau, D. L. A., Koplitz, S. N., Jacob, D. J.,
718 Mickley, L. J., Margono, B. A., and Myers, S. S.: Regional air quality impacts of
719 future fire emissions in Sumatra and Kalimantan, *Environmental Research*
720 *Letters*, 5, 054010 pp., 2015b.

721 Mauderly, J. L., and Chow, J. C.: Health effects of organic aerosols, *Inhalation*
722 *Toxicology*, 20, 257-288, 2008.

723 McBride, J. L., Haylock, M. R., and Nicholls, N.: Relationships between the Maritime
724 Continent Heat Source and the El Niño–Southern Oscillation Phenomenon,
725 *Journal of Climate*, 16, 2905-2914, 10.1175/1520-
726 0442(2003)016<2905:RBTMCH>2.0.CO;2, 2003.

727 Page, S. E., Siegert, F., Rieley, J. O., Boehm, H.-D. V., Jaya, A., and Limin, S.: The amount
728 of carbon released from peat and forest fires in Indonesia during 1997,
729 *Nature*, 420, 61-65, 2002.

730 Randerson, J. T., Chen, Y., van der Werf, G. R., Rogers, B. M., and Morton, D. C.: Global
731 burned area and biomass burning emissions from small fires, *Journal of*
732 *Geophysical Research: Biogeosciences*, 117, G04012,
733 10.1029/2012JG002128, 2012.

734 Rasmusson, E. M., and Wallace, J. M.: Meteorological Aspects of the El Niño/Southern
735 Oscillation, *Science*, 222, 1195-1202, 10.1126/science.222.4629.1195, 1983.

736 Reddington, C. L., Yoshioka, M., Balasubramanian, R., Ridley, D., Toh, Y. Y., Arnold, S.
737 R., and Spracklen, D. V.: Contribution of vegetation and peat fires to
738 particulate air pollution in Southeast Asia, *Environmental Research Letters*,
739 9, 094006, 2014.

740 Reid, J. S., Xian, P., Hyer, E. J., Flatau, M. K., Ramirez, E. M., Turk, F. J., Sampson, C. R.,
741 Zhang, C., Fukada, E. M., and Maloney, E. D.: Multi-scale meteorological
742 conceptual analysis of observed active fire hotspot activity and smoke optical
743 depth in the Maritime Continent, *Atmos. Chem. Phys.*, 12, 2117-2147,
744 10.5194/acp-12-2117-2012, 2012.

745 Reid, J. S., Lagrosas, N. D., Jonsson, H. H., Reid, E. A., Sessions, W. R., Simpas, J. B., Uy,
746 S. N., Boyd, T. J., Atwood, S. A., Blake, D. R., Campbell, J. R., Cliff, S. S., Holben, B.
747 N., Holz, R. E., Hyer, E. J., Lynch, P., Meinardi, S., Posselt, D. J., Richardson, K. A.,
748 Salinas, S. V., Smirnov, A., Wang, Q., Yu, L., and Zhang, J.: Observations of the
749 temporal variability in aerosol properties and their relationships to
750 meteorology in the summer monsoonal South China Sea/East Sea: the scale-
751 dependent role of monsoonal flows, the Madden–Julian Oscillation, tropical
752 cyclones, squall lines and cold pools, *Atmos. Chem. Phys.*, 15, 1745-1768,
753 10.5194/acp-15-1745-2015, 2015.

754 Saji, N. H., Goswami, B. N., Vinayachandran, P. N., and Yamagata, T.: A dipole mode in
755 the tropical Indian Ocean, *Nature*, 401, 360-363, 1999.

756 See, S. W., Balasubramanian, R., and Wang, W.: A study of the physical, chemical, and
757 optical properties of ambient aerosol particles in Southeast Asia during hazy
758 and nonhazy days, *Journal of Geophysical Research: Atmospheres*, 111,
759 D10S08, 10.1029/2005JD006180, 2006.

760 Seinfeld, J., and Pandis, S.: Atmospheric Physics and Chemistry. From Air Pollution to
761 Climate Change, Second Edition ed., New York (NY): JohnWiley & Sons, 2006.
762 Sekiguchi, M., Nakajima, T., Suzuki, K., Kawamoto, K., Higurashi, A., Rosenfeld, D.,
763 Sano, I., and Mukai, S.: A study of the direct and indirect effects of aerosols
764 using global satellite data sets of aerosol and cloud parameters, Journal of
765 Geophysical Research: Atmospheres, 108, 4699, 10.1029/2002JD003359,
766 2003.

767 Smith, A., Lott, N., and Vose, R.: The Integrated Surface Database: Recent
768 Developments and Partnerships, Bulletin of the American Meteorological
769 Society, 92, 704-708, doi:10.1175/2011BAMS3015.1, 2011.

770 Stauffer, D. R., and Seaman, N. L.: Multiscale Four-Dimensional Data Assimilation,
771 Journal of Applied Meteorology, 33, 416-434, 10.1175/1520-
772 0450(1994)033<0416:mfdada>2.0.co;2, 1994.

773 Tosca, M. G., Randerson, J. T., Zender, C. S., Nelson, D. L., Diner, D. J., and Logan, J. A.:
774 Dynamics of fire plumes and smoke clouds associated with peat and
775 deforestation fires in Indonesia, Journal of Geophysical Research:
776 Atmospheres, 116, n/a-n/a, 10.1029/2010JD015148, 2011.

777 van der Werf, G. R., Randerson, J. T., Giglio, L., Collatz, G. J., Mu, M., Kasibhatla, P. S.,
778 Morton, D. C., DeFries, R. S., Jin, Y., and van Leeuwen, T. T.: Global fire
779 emissions and the contribution of deforestation, savanna, forest, agricultural,
780 and peat fires (1997–2009), Atmos. Chem. Phys., 10, 11707-11735,
781 10.5194/acp-10-11707-2010, 2010.

782 Visscher, A. D.: Air Dispersion Modeling: Foundations and Applications, First ed.,
783 John Wiley & Sons, Inc., 2013.

784 Wang, J., Ge, C., Yang, Z., Hyer, E. J., Reid, J. S., Chew, B.-N., Mahmud, M., Zhang, Y., and
785 Zhang, M.: Mesoscale modeling of smoke transport over the Southeast Asian
786 Maritime Continent: Interplay of sea breeze, trade wind, typhoon, and
787 topography, Atmospheric Research, 122, 486-503,
788 <http://dx.doi.org/10.1016/j.atmosres.2012.05.009>, 2013.

789 Wiedinmyer, C., Akagi, S. K., Yokelson, R. J., Emmons, L. K., Al-Saadi, J. A., Orlando, J. J.,
790 and Soja, A. J.: The Fire INventory from NCAR (FINN): a high resolution global
791 model to estimate the emissions from open burning, Geosci. Model Dev., 4,
792 625-641, 10.5194/gmd-4-625-2011, 2011.

793 Wu, C.-H., and Hsu, H.-H.: Topographic Influence on the MJO in the Maritime
794 Continent, Journal of Climate, 22, 5433-5448, 10.1175/2009JCLI2825.1,
795 2009.

796 Wu, R., Wen, Z., and He, Z.: ENSO Contribution to Aerosol Variations over the
797 Maritime Continent and the Western North Pacific during 2000–10, Journal
798 of Climate, 26, 6541-6560, 10.1175/JCLI-D-12-00253.1, 2013.

799 Zhang, C.: Madden-Julian Oscillation, Reviews of Geophysics, 43, RG2003,
800 10.1029/2004RG000158, 2005.

802

803
804

Table 1. WRF physics scheme configuration

Physics Processes	Scheme
microphysics	Morrison (2 moments) scheme
longwave radiation	rrtmg scheme
shortwave radiation	rrtmg scheme
surface-layer	MYNN surface layer
land surface	Unified Noah land-surface model
planetary boundary layer	MYNN 2.5 level TKE scheme
cumulus parameterization	Grell-Freitas ensemble scheme

805
806
807
808

809 Table 2. Annual mean low visibility days (LVDs; observed visibility ≤ 10 km) and very
810 low visibility days (VLVDs; observed visibility ≤ 7 km) per year in Bangkok, Kuala
811 Lumpur, Singapore and Kuching during 2003-2014 are presented in the second column.
812 Parentheses show the percentage of year. The third column shows the percentages, along
813 with standard deviations, of low visibility days explained by fire aerosols alone (i.e. the
814 LVDs captured by the model). The fourth column is the same as the third column but for
815 non-fire (other) pollutions, which is calculated as 100% - fire pollution contribution (i.e.
816 the percentage of LVDs not captured by the model).
817

FNL_FINN	LVD per year (days)	Fire pollution contribution (%)	Other pollution contribution (%)
Bangkok, Thailand	215±50 (59±14%)	39±8	61±8
Kuala Lumpur, Malaysia	174±78 (48±21%)	36±17	64±17
Singapore, Singapore	96±87 (26±24%)	34±17	66±17
Kuching, Malaysia	95±57 (26±17%)	33±15	67±15
FNL_FINN	VLVD per year (days)	Fire pollution contribution (%)	Other pollution contribution (%)
Bangkok, Thailand	15±8 (4±2%)	87±20	13±20
Kuala Lumpur, Malaysia	19±18 (5±5%)	85±17	15±17
Singapore, Singapore	4±4 (1±1%)	91±33	9±33
Kuching, Malaysia	22±18 (6±5%)	93±11	7±11
ERA_FINN	LVD per year (days)	Fire pollution contribution (%)	Other pollution contribution (%)
Bangkok, Thailand	215±50 (59±14%)	46±7	54±7
Kuala Lumpur, Malaysia	174±78 (48±21%)	40±16	60±16
Singapore, Singapore	96±87 (26±24%)	37±18	63±18
Kuching, Malaysia	95±57 (26±17%)	45±17	55±17
ERA_FINN	VLVD per year (days)	Fire pollution contribution (%)	Other pollution contribution (%)
Bangkok, Thailand	15±8 (4±2%)	88±20	12±20
Kuala Lumpur, Malaysia	19±18 (5±5%)	90±18	10±18
Singapore, Singapore	4±4 (1±1%)	98±6	2±6
Kuching, Malaysia	22±18 (6±5%)	94±11	6±11
FNL_GFED	LVD per year (days)	Fire pollution contribution (%)	Other pollution contribution (%)
Bangkok, Thailand	215±50 (59±14%)	36±8	64±8
Kuala Lumpur, Malaysia	174±78 (48±21%)	28±17	72±17
Singapore, Singapore	96±87 (26±24%)	29±21	71±21
Kuching, Malaysia	95±57 (26±17%)	26±18	74±18
FNL_GFED	VLVD per year (days)	Fire pollution contribution (%)	Other pollution contribution (%)
Bangkok, Thailand	15±8 (4±2%)	90±19	10±19
Kuala Lumpur, Malaysia	19±18 (5±5%)	83±28	17±28
Singapore, Singapore	4±4 (1±1%)	89±37	11±37
Kuching, Malaysia	22±18 (6±5%)	89±28	11±28

818

819 Table 3. Annual mean and standard deviation of modeled fire PM_{2.5} concentration (µg m⁻³)
820 ³) in Bangkok, Kuala Lumpur, Singapore, and Kuching during 2003-2014 contributed by
821 each source region (s1 – s5). Parentheses show the percentage of fire PM_{2.5} contribution
822 originating from each source region. Regions s1-s5 are defined in Fig. 1. FNL_FINN,
823 ERA_FINN and FNL_GFED are three model simulations described in Section 2.1.
824

FNL_FINN	s1	s2	s3	s4	s5
Bangkok	8.4±2.3 (99.2±0.5%)	0.0±0.0 (0.1±0.1%)	0.0±0.0 (0.1±0.1%)	0.1±0.0 (0.6±0.5%)	0.0±0.0 (0.0±0.0%)
Kuala Lumpur	2.3±1.2 (43.3±14.8%)	2.7±1.4 (49.6±14.9%)	0.2±0.2 (3.3±3.4%)	0.1±0.1 (2.5±2.3%)	0.0±0.0 (0.3±0.2%)
Singapore	1.1±0.7 (36.7±14.7%)	1.2±0.8 (40.7±15.9%)	0.4±0.4 (14.3±10.0%)	0.2±0.1 (6.1±3.8%)	0.1±0.0 (2.2±1.1%)
Kuching	0.5±0.4 (7.8±6.5%)	0.3±0.1 (4.7±2.5%)	6.0±3.2 (84.6±9.7%)	0.1±0.1 (2.3±2.5%)	0.0±0.0 (0.6±0.3%)
ERA_FINN	s1	s2	s3	s4	s5
Bangkok	9.1±2.3 (99.2±0.4%)	0.0±0.0 (0.1±0.1%)	0.0±0.0 (0.1±0.1%)	0.1±0.0 (0.6±0.4%)	0.0±0.0 (0.0±0.0%)
Kuala Lumpur	2.3±1.2 (39.7±12.7%)	3.2±1.4 (53.7±12.3%)	0.2±0.2 (3.9±3.3%)	0.1±0.0 (2.3±1.8%)	0.0±0.0 (0.4±0.2%)
Singapore	1.1±0.6 (34.2±13.5%)	1.4±0.9 (40.5±13.7%)	0.6±0.6 (17.2±11.8%)	0.2±0.1 (6.2±3.1%)	0.1±0.0 (1.9±0.9%)
Kuching	0.5±0.4 (8.1±5.6%)	0.4±0.2 (6.1±3.9%)	6.7±3.9 (82.5±10.0%)	0.1±0.1 (2.7±3.0%)	0.0±0.0 (0.6±0.3%)
FNL_GFED	s1	s2	s3	s4	s5
Bangkok	4.8±1.3 (99.6±0.2%)	0.0±0.0 (0.1±0.0%)	0.0±0.0 (0.1±0.1%)	0.0±0.0 (0.2±0.2%)	0.0±0.0 (0.1±0.0%)
Kuala Lumpur	1.3±0.6 (38.6±20.8%)	2.7±1.9 (53.8±21.1%)	0.1±0.2 (2.8±3.5%)	0.0±0.0 (0.8±0.8%)	0.1±0.1 (3.9±3.4%)
Singapore	0.3±0.2 (22.1±17.3%)	1.5±1.8 (40.2±23.6%)	0.4±0.5 (12.5±9.5%)	0.1±0.0 (2.9±2.4%)	0.4±0.2 (22.3±13.2%)
Kuching	0.1±0.1 (7.2±6.8%)	0.1±0.1 (4.3±3.2%)	3.2±3.2 (75.2±12.9%)	0.0±0.0 (1.7±2.7%)	0.3±0.2 (11.6±6.7%)

825
826

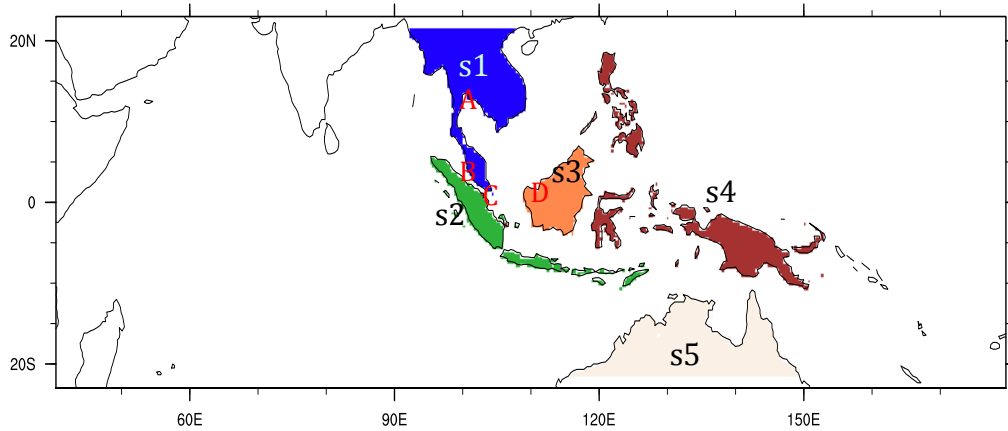
827 Table 4. The spatial and temporal correlation of monthly rainfall between models
 828 (FNL_FINN and ERA_FINN) and observation (TRMM) during 2003-2014. FMA, MJJ,
 829 ASO, NDJ and All represents February-April, May-July, August-October, November-
 830 January and whole year, respectively.

831

	FNL_FINN vs. TRMM		ERA_FINN vs. TRMM	
	Spatial cor.	Temporal cor.	Spatial cor.	Temporal cor.
FMA	0.89	0.61	0.89	0.89
MJJ	0.83	0.69	0.81	0.90
ASO	0.86	0.59	0.84	0.89
NDJ	0.88	0.60	0.88	0.85
All	0.86	0.68	0.85	0.90

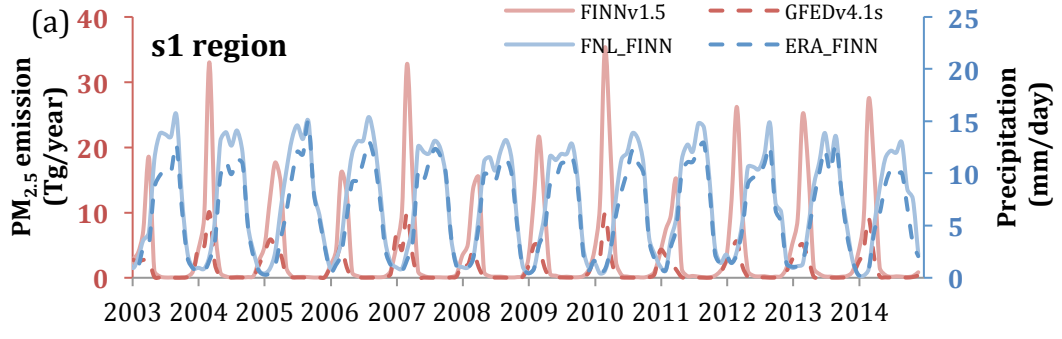
832

833

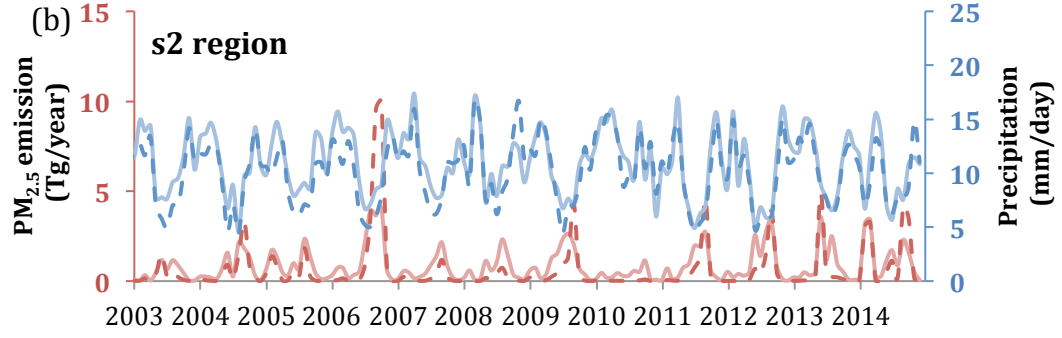


834
 835
 836
 837
 838
 839
 840
 841

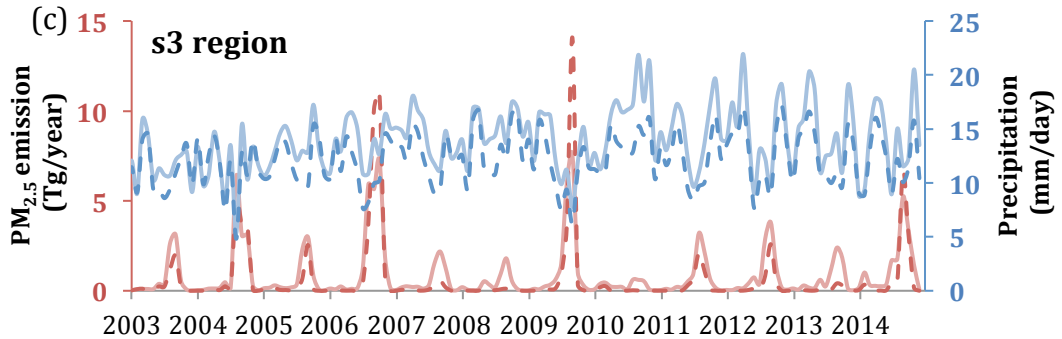
Figure 1. Model domain used for simulations. The domain has 432×148 grid points with a horizontal resolution of 36 km. Five fire source regions marked in different colors and labeled as s1, s2, s3, s4 and s5, represent mainland Southeast Asia (s1), Sumatra and Java islands (s2), Borneo (s3), the rest of Maritime Continent (s4), and northern Australia (s5). A, B, C and D indicate the location of four selected cities: Bangkok (A), Kuala Lumpur (B), Singapore (C) and Kuching (D).



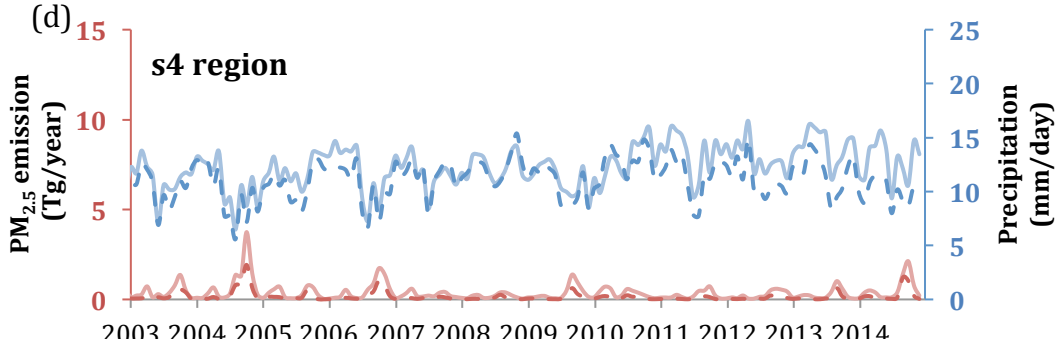
842



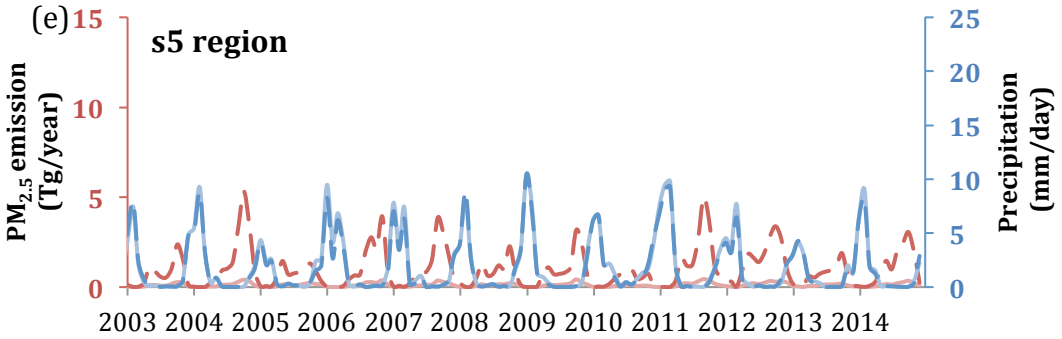
843



844



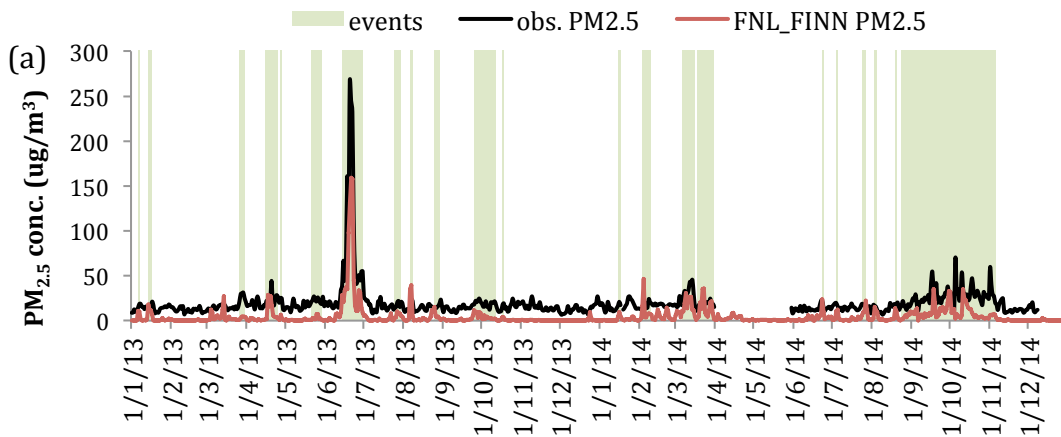
845



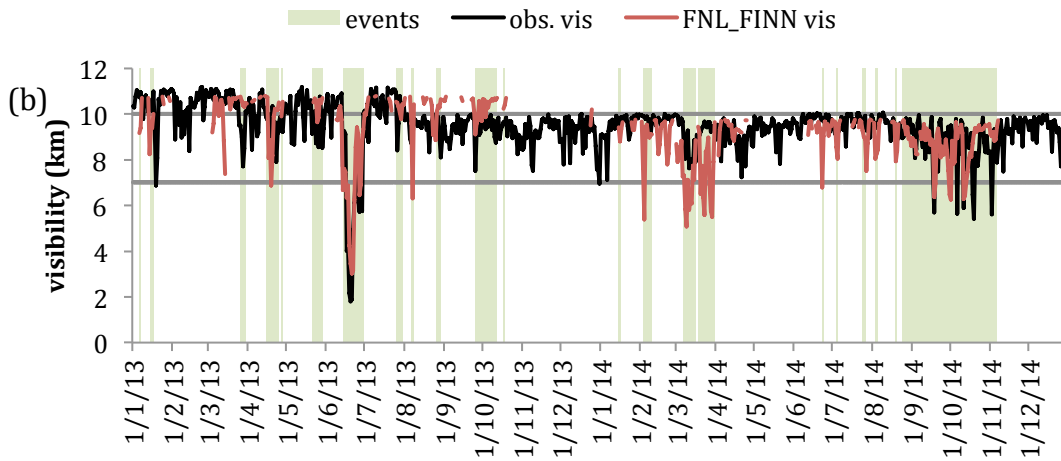
846

847 Figure 2. Time series of monthly $PM_{2.5}$ emission ($Tg\ year^{-1}$) in FINNv1.5 (pink solid
848 lines) and GFEDv4.1s (red dashed lines). Also shown are precipitation rates ($mm\ day^{-1}$)
849 simulated in FNL_FINN (light blue solid lines) and ERA_FINN (blue dashed lines)
850 during 2003-2014 in: (a) mainland Southeast Asia (s1), (b) Sumatra and Java islands (s2),
851 (c) Borneo (s3), (d) the rest of the Maritime Continent (s4), and (e) northern Australia
852 (s5).
853

854



855



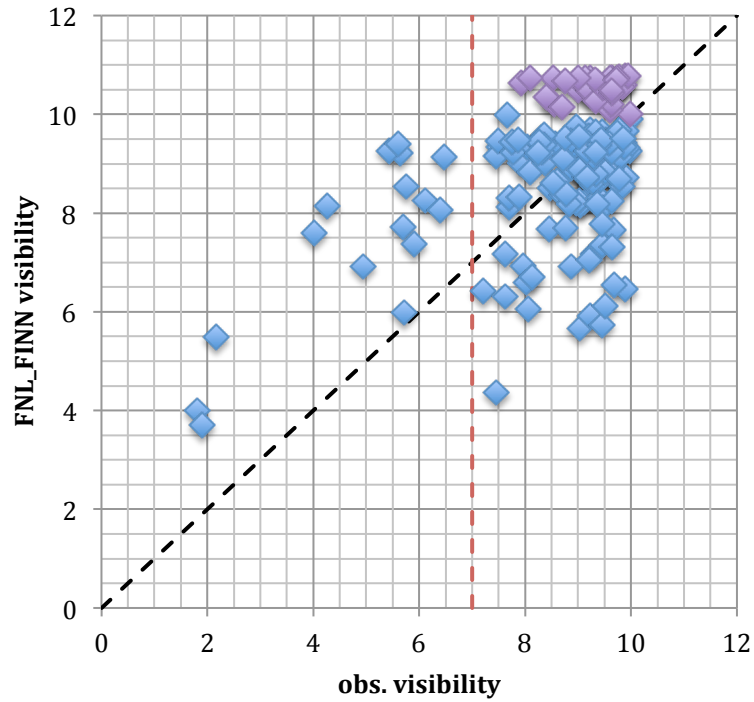
856

857

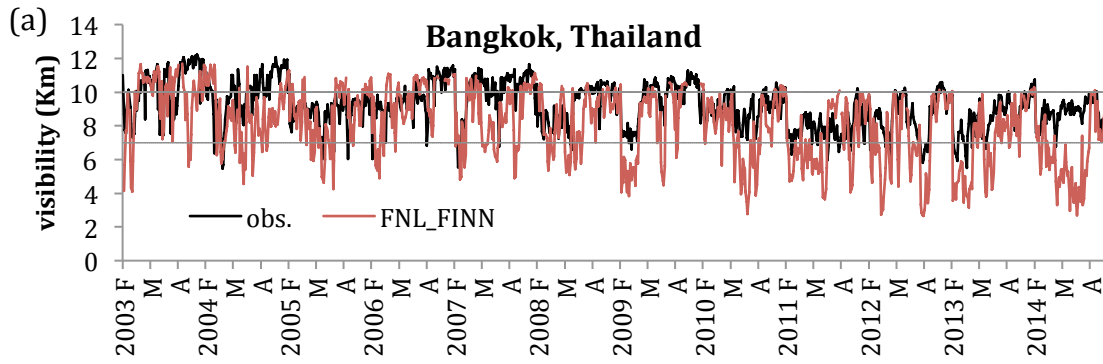
858 Figure 3. (a) Time series of daily surface $PM_{2.5}$ from the ground-based observations
859 (black line) and FNL_FINN simulated results (red line) in Singapore during 2013-2014.
860 (b) Same as (a) but daily visibility from GSOD observations (black line) and calculated
861 result from FNL_FINN (red line). Highlighted green areas are known haze events caused
862 by fire aerosols, which are reported by news or manually selected based on observed
863 $PM_{2.5}$. Two gray lines mark the visibility of 7 and 10 km, respectively.

864

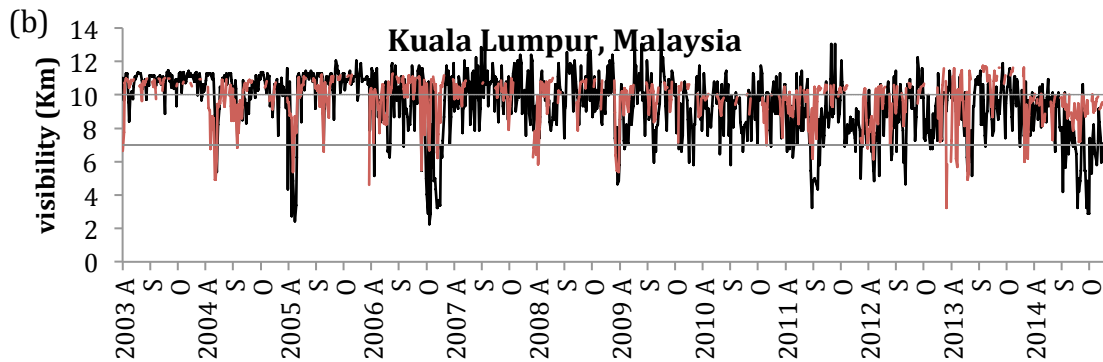
865



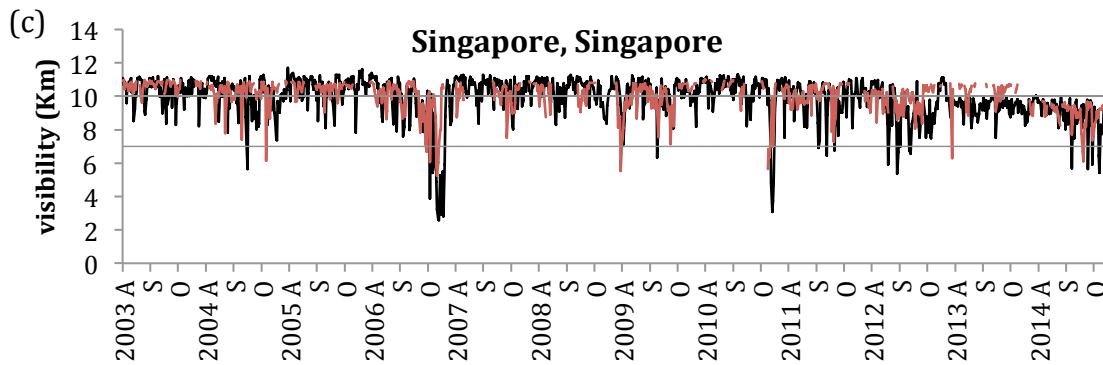
866
867 Figure 4. A scatter plot of observed visibility and FNL_FINN visibility during known fire
868 events as labeled in Fig. 3b. Black dash line refers 1:1 line and red line is the threshold of
869 VLVD (7 km). Purple points remark the known low visibility events that model failed to
870 produce a visibility at least qualified for LVD.
871



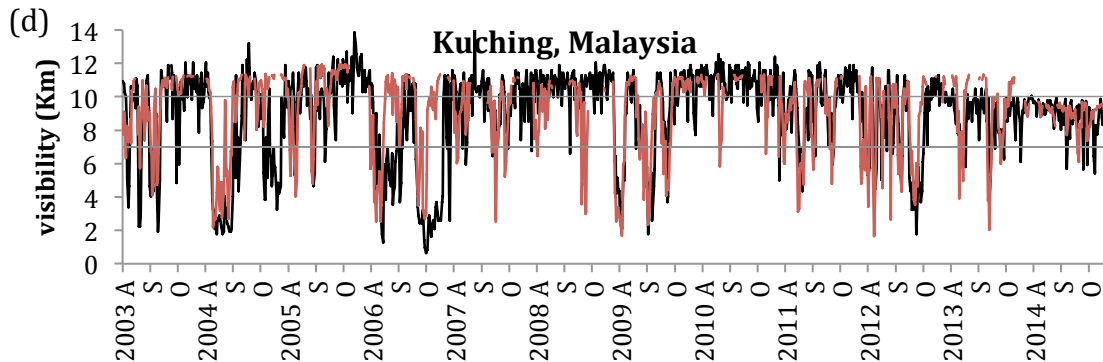
872



873



874

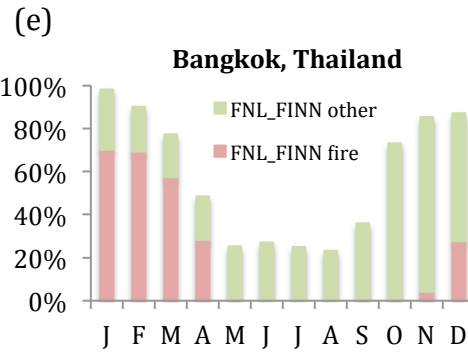
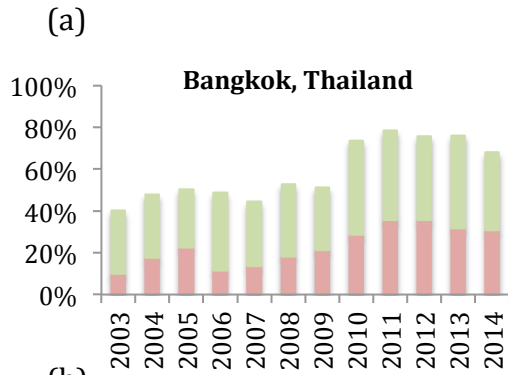


875

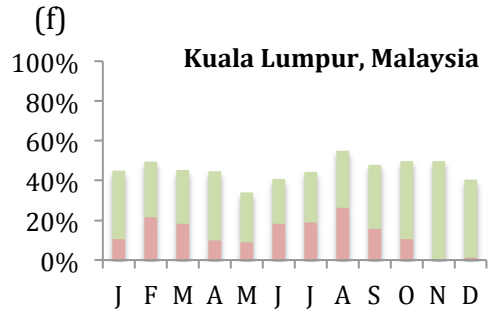
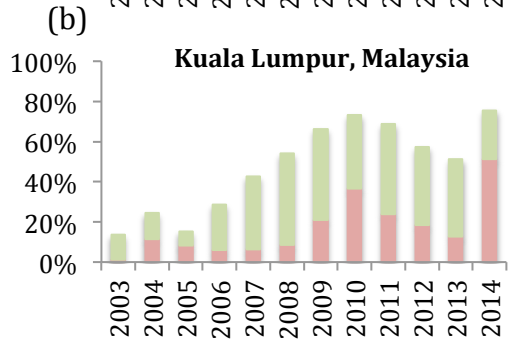
876 Figure 5. Comparison of daily visibility between GSOD observation (black lines) and
 877 FNL_FINN modeled result (red lines) in: (a) Bangkok, (b) Kuala Lumpur, (c) Singapore,
 878 (d) Kuching during the fire seasons from 2003 to 2014. Two grey lines mark the visibility
 879 of 7 and 10 km, respectively. F, M and A in the x-axis of (a) indicates February, March

880 and April, respectively. A, S and O in the x-axis of (b) – (d) are August, September, and
881 October, respectively.
882

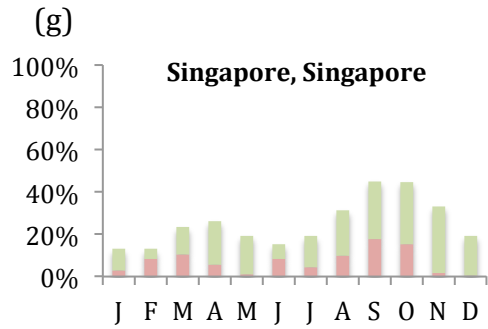
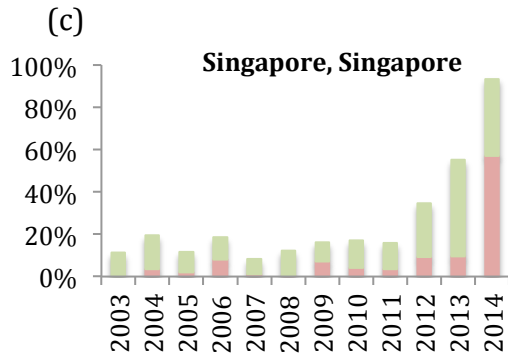
883



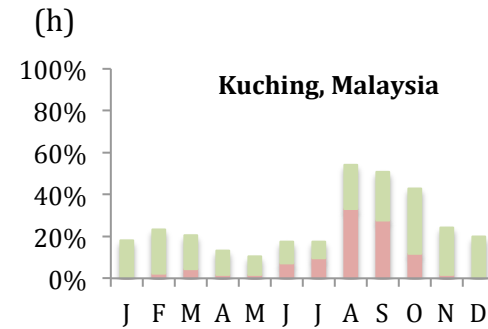
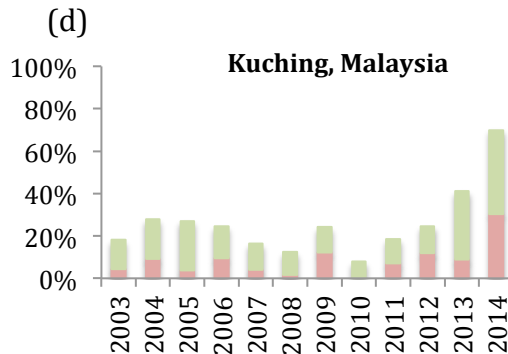
884



885



886



887

888

889

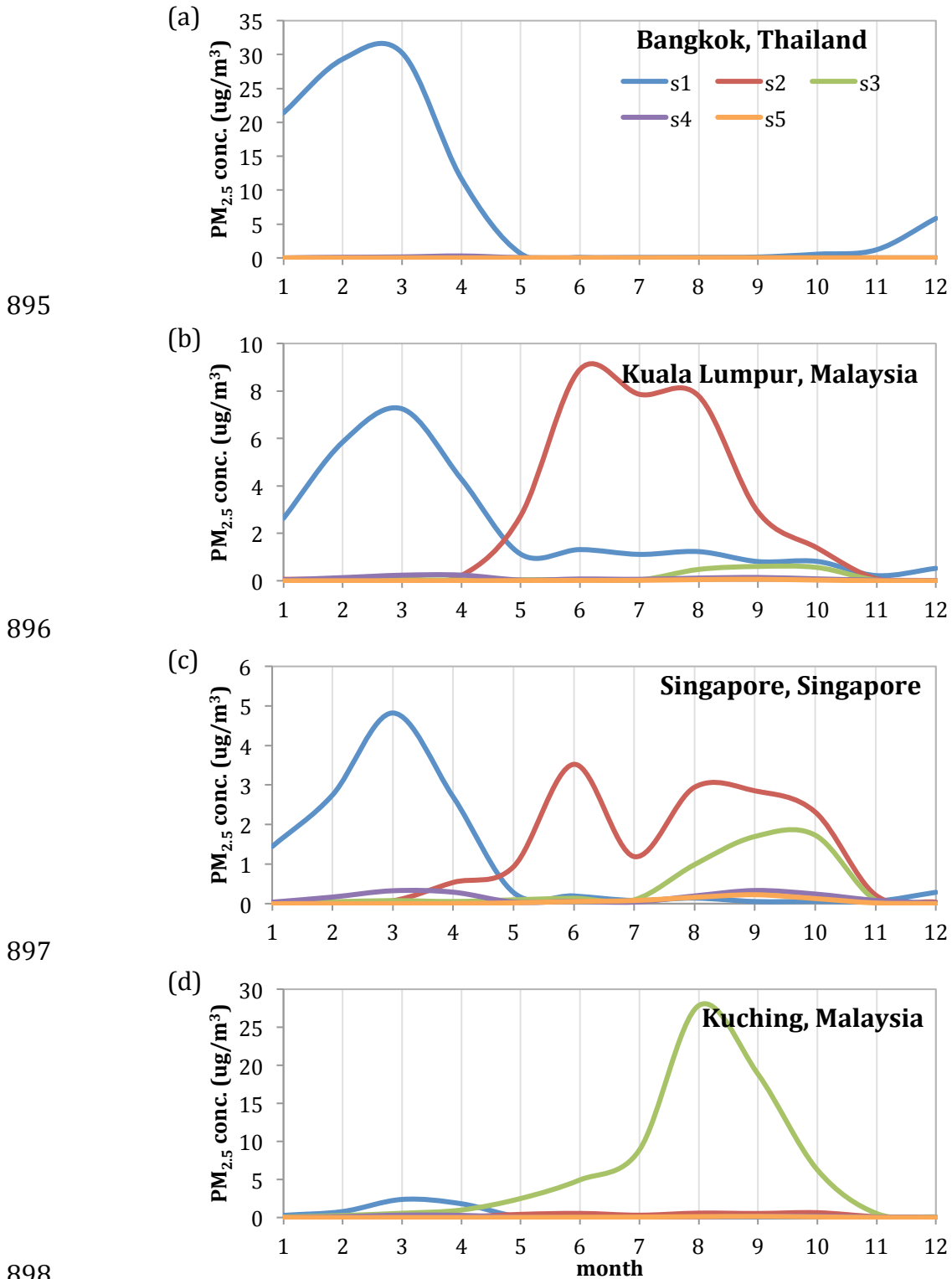
890

891

892

Figure 6. (a) – (d) The percentage of LVDs per year derived using from GSOD visibility observations in Bangkok, Kuala Lumpur, Singapore, and Kuching, respectively. (e) – (h) The percentage of LVDs averaged over 2003-2014, derived using GSOD visibility observations in Bangkok, Kuala Lumpur, Singapore, and Kuching, respectively. Each bar presents the observed LVDs in each year or month. Red color shows the partition of fire-

893 caused LVDs (captured by model) while green color presents other LVDs (observed –
894 modeled; i.e. those not captured by model).



895

896

897

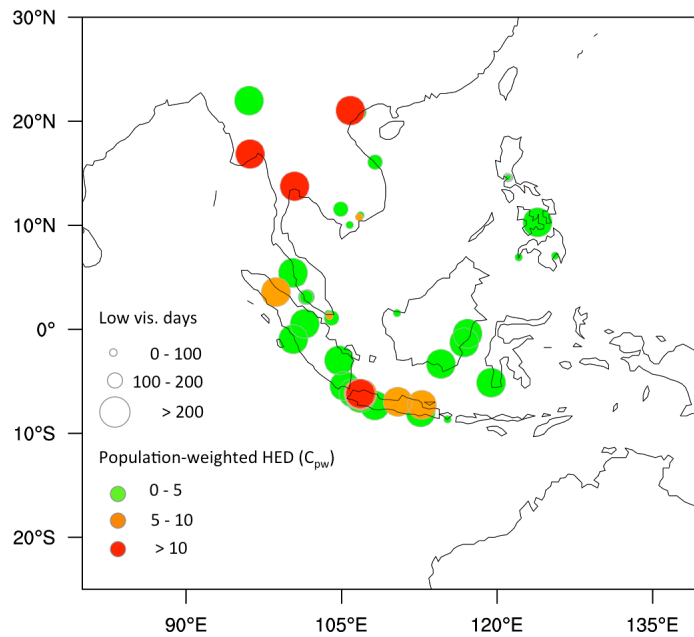
898

899

900 Figure 7. The mean fire $PM_{2.5}$ concentrations within the PBL attributed to different
 901 emission regions (s1 - s5) in (a) Bangkok, (b) Kuala Lumpur, (c) Singapore and (d)
 902 Kuching, all derived from FNL_FINN simulation and averaged over the period of 2003-
 903 2014.

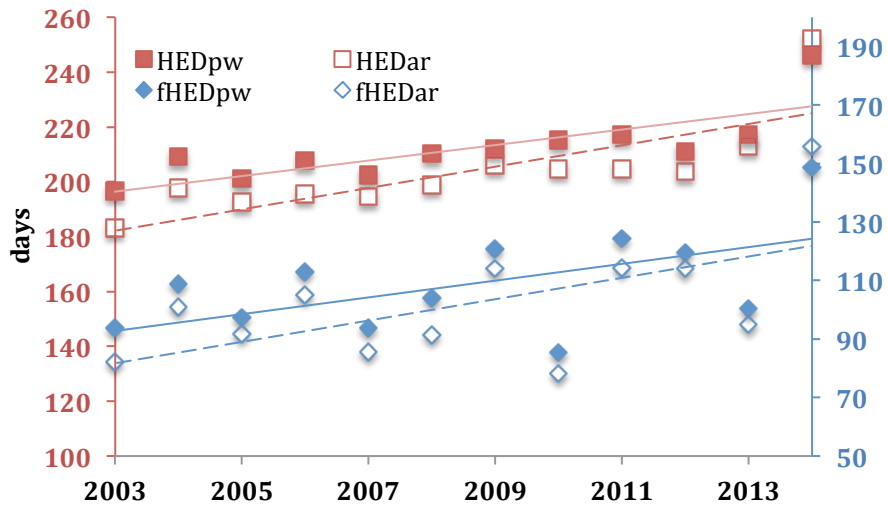
904

(a)



905

(b)



906

907

908

909

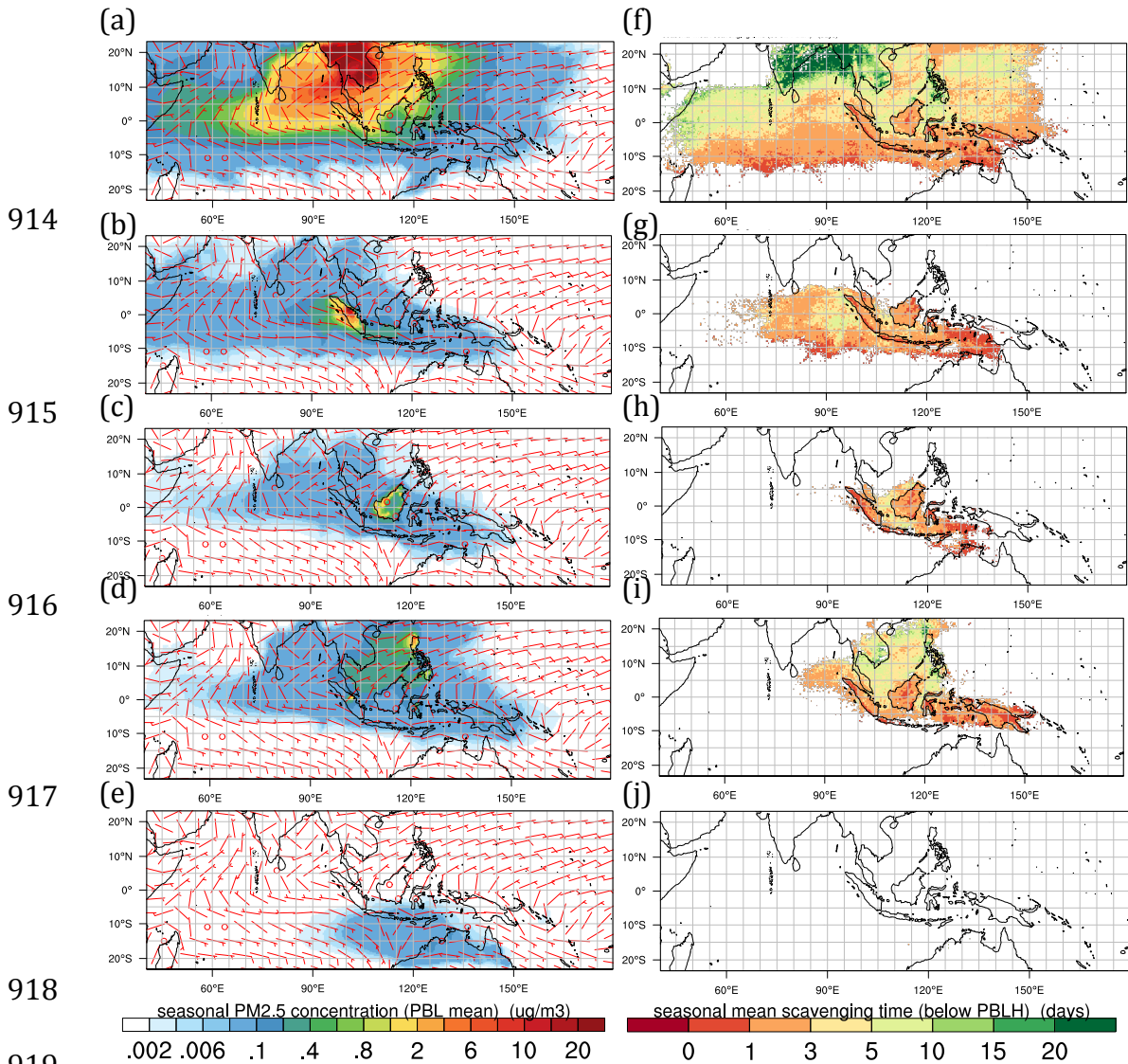
910

911

912

913

Figure 8. (a) The mean low visibility days (circles) per year from 2003 to 2014 in 50 ASEAN cities. The size of the circles indicates the number of days. The colors refer to population-weighted fraction in the total Haze Exposure Days (HED). (b) Annual population-weighted HED (HED_{pw}) and arithmetic mean HED (HED_{ar}). Fire-caused HED are labeled as $fHED_{pw}$ and $fHED_{ar}$. Units are in days. Note that the y-axes are in different scales.



919 Figure 9. Seasonal mean fire $\text{PM}_{2.5}$ concentration ($\mu\text{g m}^{-3}$) and wind within the PBL
 920 modeled in FNL_FINN during February to April, 2003–2014 for fire $\text{PM}_{2.5}$ source region
 921 from (a) mainland Southeast Asia, (b) Sumatra and Java islands, (c) Borneo, (d) the rest
 922 of the Maritime Continent, and (e) northern Australia. (f)-(j) Same as (a)-(e) but for
 923 seasonal mean wet scavenging time (days).
 924
 925